

Geochemistry of Permian Rocks from the Margins of the Phosphoria Basin: Lakeridge Core, Western Wyoming

By

Robert B. Perkins¹, Brandie McIntyre², James R. Hein², and David Z. Piper¹

Open-File Report 03–21

2003

This report is preliminary and has not been reviewed for conformity with U.S. Geological Survey editorial standards or with the North American Stratigraphic Code. Any use of trade, firm, or product names is for descriptive purposes only and does not imply endorsement by the U.S. Government.

**U.S. DEPARTMENT OF THE INTERIOR
U.S. GEOLOGICAL SURVEY**

¹ U.S. Geological Survey, MS 901, 345 Middlefield Rd, Menlo Park, CA 942025

² U.S. Geological Survey, MS 999, 345 Middlefield Rd, Menlo Park, CA 942025

CONTENTS

ABSTRACT	1
INTRODUCTION	1
BACKGROUND	2
Oceanographic Setting of the Phosphoria Basin	2
Stratigraphic Relationships	3
Lakeridge Core	5
Previous Studies of the Lakeridge Core	6
SAMPLING AND ANALYTICAL METHODS	7
Sample Selection and Preparation	7
Geochemical Analyses and Data Evaluation	8
RESULTS AND DISCUSSION	10
CALCULATION OF NORMATIVE SEDIMENTARY COMPONENTS	10
ELEMENTAL PARTITIONING	12
Temporal Variations in Geochemistry	15
Terrigenous Elements	15
Marine Elements	18
Variations in Trace Element Concentrations	23
SUMMARY CONCLUSIONS	24
ACKNOWLEDGEMENTS	26
REFERENCES	26

FIGURES

Figure 1. Map showing location of Lakeridge core in context of Permian paleogeography with present latitude and longitude coordinates. The eastern and northern extent of the Phosphoria Basin is shown by bold line. Major tectonic features include the remnant Antler Highlands to the west, the Ancestral Front Range to the southeast, and the Milk River Uplift to the north. The Phosphoria Basin is separated from shallow, evaporite basins in eastern Wyoming, North and South Dakota, and Nebraska by a carbonate platform lying east of the Lakeridge section.

Figure 2. Position of the Lakeridge section on the upper slopes of a low-angle carbonate ramp and generalized lithologic relationships of the Park City Formation (PCF) and Phosphoria Formation (PF) (modified from Burchette and Wright, 1992 and Maughan, 1994).

Figure 3. Generalized stratigraphic column of the Park City Formation (PCF), Phosphoria Formation, and Shedhorn Sandstone in the Lakeridge core. Series and stage names from Ross and Ross (1995). B = burrowed; Biocl = bioclastic; Brc = brecciated; Ev = evaporates; F = fossiliferous; Ph = phosphatic; Py = pyritic; V = vuggy.

Figure 4. Scatter plots showing major-element oxides that occur almost exclusively in the terrigenous fraction (Al_2O_3 , Fe_2O_3 , K_2O , TiO_2) and others that occur dominantly in other phases but also in the terrigenous fraction (Na_2O , and SiO_2). The detrital Al_2O_3 content (15.1%) is calculated based on extrapolation of the maxima (mixing) line in the CaO vs Al_2O_3 plot to near-zero percent CaO ; see text for discussion of minima, maxima, and regression lines.

Figure 5. Variations in rock composition with stratigraphic position in the Lakeridge core. Component fractions determined from major-element oxide concentrations. Background shadings denote stratigraphic units. Missing core intervals (see fig. 3) split between overlying and underlying beds. MPM is Meade Peak Member.

Figure 6. Scatter plots showing relationships between select marine elements. Note difference in Cd:Zn and Mo:Zn x-axis scales. Lines represent average ratios in modern deep seawater (SW) and modern marine plankton (MP).

Figure 7. Scatter plots showing relationships between select marine elements and total organic carbon (TOC) and sulfur. Note sharp maxima lineation of points in element vs S plots.

Figure 8. Variations in selected terrigenous element vs alumina ratios with stratigraphic position in the Lakeridge core. Solid vertical lines denote major-element oxide ratios for world shale average (Turekian and Wedepohl, 1961; Wedepohl, 1969-78). "SS" denotes Shedhorn Sandstone beds.

Figure 9. Variations in select marine element and element-oxide ratios and Ce anomalies with stratigraphic position in the Lakeridge core. Solid vertical lines denote seawater ratios; dashed vertical lines represent average marine plankton ratios (Martin and Knauer, 1973; Collier and Edmond, 1984; Collier, 1985; Brumsack, 1986); dotted vertical line represents

WSA value for REEs (Piper, 1974). Blank areas (e.g., in Franson) represent intervals in which total concentration of one or both elements was below detection limits or marine fractions were insignificant. “SS” denotes Shedhorn Sandstone beds.

Figure 10. Variations in selected trace element concentrations with stratigraphic position in the Lakeridge core. Dotted vertical lines represent world shale average (Turekian and Wedepohl, 1961; Wedepohl, 1969-78). Blank areas in Cd plot are intervals where Cd concentrations were below detection limits.

TABLES

Table 1a. Summary of Lakeridge core analytical data from Medrano and Piper (1995). Samples from the Grandeur Member of the Park City Formation were not analyzed. Major element oxides and F in wt. %; all others in mg kg^{-1} .

Table 1b. Previously unreported selenium concentrations for Medrano and Piper (1995) samples.

Table 2. X-ray diffraction mineralogy of selected samples.

Table 3a. Quality control limits for the analytical techniques used in this study.

Table 3b. Correlation coefficients for analytes measured by two different analytical techniques.

Table 4. Major-element oxide and F, C, and S concentrations.

Table 5. Minor-element concentrations in mg kg^{-1} ; “<” indicates less than the detection limit given.

Table 6. Selected rare earth element and Y concentrations in mg kg^{-1} .

Table 7. Gold, platinum, and palladium concentrations ($\mu\text{g kg}^{-1}$) in select samples.

Table 8. Correlation coefficients for the log concentrations of major and minor elements.

Table 9. World shale average, modern marine plankton, and seawater concentrations of selected elements.

Table 10. Formulas used to calculate the normative components from measured major-element oxide contents (wt %).

Table 11. Major components in composite samples from the Lakeridge core. All values in wt %, calculated from major-element-oxide contents and the formulas in Table 9.

Table 12. Principal component analysis of log-normalized concentration data from Lakeridge core samples. Orthogonal varimax transformation using StatView™ software. Values of 0.40 or greater are in bold.

ABSTRACT

The Permian Phosphoria Formation and interbedded units of the Park City Formation and Shedhorn Sandstone in western Wyoming represent deposition along a carbonate ramp at the eastern margin of the Phosphoria Basin, with portions of the Phosphoria units reflecting periods of upwelling and widespread phosphogenesis. Thickness-weighted slab-samples of these units were collected at a maximum interval of 3 m along an 80+ m-length of unweathered core and analyzed for major-, minor-, and trace-element contents.

Interpretations of geochemistry were made within the confines of a previously recognized sequence stratigraphy framework. Major shifts in element ratios characteristic of terrigenous debris that occur at sequence boundaries at the base of the Meade Peak and Retort Members of the Phosphoria Formation are attributed to changing sediment sources. Inter-element relationships in the marine fraction indicate that bottom waters of the Phosphoria Basin were predominantly denitrifying during deposition of the Ervay, Grandeur, and Phosphoria sediments, although sulfate-reducing conditions may have existed during deposition of the lower Meade Peak sediments. Oxic conditions were prevalent during deposition of a large part of the Franson Member, which represents sedimentation in a shallow, inner- to back-ramp setting.

Variations in sediment facies and organic matter and trace element contents largely reflect changes in Permian sea level. Changes in sea level in basin-margin areas, such as represented by the study section, may have affected the oxidation of settling organic matter, the foci of intersection of upwelling bottom waters with the photic zone, the rate of terrigenous sedimentation, and, ultimately, the overall environment of deposition. Our study suggests that phosphogenesis can occur under lowstand, transgressive, and highstand conditions in marginal areas, assuming water depths sufficient for upwelling to occur. Formation of phosphorite layers under upwelling conditions appears to have been most dependent on a lack of dilution by terrigenous sedimentation and carbonate shoaling. Differences in the geochemistry between two similar environments represented by the upper and lower Phosphoria units are largely attributed to higher rates of diluting terrigenous sediment during deposition of the upper unit. This is consistent with prior interpretations of a more shoreward setting for the upper Phosphoria.

INTRODUCTION

The Permian Phosphoria and Park City Formations are marine sedimentary deposits that extend over several 100,000 km² in eastern Idaho, southwestern Montana, northern Utah, and western to central Wyoming (McKelvey and others, 1959). The Phosphoria Formation is of economic importance as a source of phosphate in North America, containing as much as 50 tons m⁻² of apatite through the most phosphate-enriched sections (Gulbrandsen and Krier, 1980; Piper, 2001). It also contains relatively high concentrations of many trace elements (Vine and Tourtelot, 1970), some of which

are of environmental concern. The Phosphoria and Park City Formations record marine paleoenvironmental conditions along the western margin of Pangea at the end of the Paleozoic.

Despite decades of scientific study, many aspects of the paleoceanographic and phosphogenic processes that gave rise to the Phosphoria Formation are still unclear. Part of the problem in unraveling the geologic history recorded by the Phosphoria Formation is the lack of continuous, accessible, and unweathered stratigraphic sections. This is especially true for phosphatic shale units, which are easily weathered.

In this study, we examine the geochemistry and lithology of a nearly continuous section of the Phosphoria Formation and interbedded units of the Park City Formation and Shedhorn Sandstone. This cored section was obtained from General Petroleum's Lakeridge No. 43-19-G well in western Wyoming from depths exceeding 4,300 m. The core, originally described by Sheldon (1963), represents an unweathered geochemical record of marine conditions through the upper Permian along the shoreward margin of the Phosphoria Basin.

Our objectives are to use interelement relationships to define paleoenvironmental characteristics (e.g., paleoproductivity, bottom-water redox conditions), to relate temporal changes in these calculated parameters to lithologic variability in the context of previously proposed sequence stratigraphic models, and to elucidate the primary controls on the accumulation of apatite and trace elements.

BACKGROUND

Oceanographic Setting of the Phosphoria Basin

The Phosphoria and Park City Formations accumulated in a terrigenous sediment-starved basin on the outer margin of the Wyoming-Idaho epicratonic platform after the final phases of Pennsylvanian and Early Permian ancestral Rocky Mountain tectonism (Maughan, 1984; Tisoncik, 1984). The depocenter of the Phosphoria Sea, an interior sag basin (Wardlaw and Collinson, 1986), was originally located between approximately 5° and 25°N paleolatitude (fig. 1; shown with present coordinates). The Phosphoria Basin was bounded to the north by the Milk River Uplift in western Montana, to the south by

the Confusion Shelf and Front Range Uplift, and to the east by the broad evaporative Goose Egg Basin in eastern Wyoming and western North Dakota and Nebraska.

The paleoshelf on which the Phosphoria and Park City Formations were deposited was nearly flat, as constrained by overall basin dimensions. Using reasonable values of approximately 400 km for basin width and 400 m for maximum depth in the western margin of the basin (McKelvey and others, 1959; Maughan, 1994; Piper and Link, 2002), the calculated shelf slope-angle is estimated to have been 0.06°. The regional occurrence of marker beds (e.g., the 10-cm thick basal “fish-scale bed”) would seem to preclude large-scale paleorelief features or shelf slope breaks. These late Permian formations were therefore deposited on a low-gradient, westward facing carbonate ramp leading from a carbonate platform separating the Phosphoria Basin from the shallow evaporative basin in the east to the basin interior (figs. 1 and 2). The Lakeridge section was located near the northeastern margin of the Phosphoria Basin, proximal to the carbonate platform and in a mid- to inner-ramp setting possibly subject to storm-induced wave-base turbulence (Burchette and Wright, 1992).

Stratigraphic Relationships

In western Wyoming, the Phosphoria Formation was deposited in two depositional sequences that intertongue with carbonate deposits of the Park City Formation. The lower Phosphoria sequence, comprised of the Meade Peak phosphatic shale and Rex Chert Members, is generally recognized as being unconformable on the underlying sandy carbonates comprising the Grandeur tongue of the Park City Formation (figs 2 and 3). Although Sheldon (1963) designated that part of the Lakeridge core underlying the Meade Peak as the Wells Formation, McKelvey and others (1959) had earlier re-assigned the upper siliceous limestones formerly considered to belong to the Wells Formation to the Grandeur Member of the Park City Formation. The lower Phosphoria sequence is overlain by a basinward projecting tongue of carbonate comprising the Franson Member of the Park City Formation. The Franson, in turn, is overlain by the upper Phosphoria sequence, composed of the Retort phosphatic shale and the Tosi chert Members. The upper Phosphoria is overlain by the carbonate-rich Ervay Member of the Park City Formation. Three intervals of carbonate-rich quartz sand,

designated the Shedhorn Sandstone, are present in the Lakeridge core, the lower and thickest layer lies between the Rex Chert and Franson, the middle within the Franson, and the upper at the base of the Ervay.

The Phosphoria and Park City Formations have been interpreted as reflecting three third-order eustatic transgressive-regressive cycles off of the Wyoming craton (Peterson, 1980; Inden and Coalson, 1996; Whalen, 1996). The boundaries between these three sequences are regional unconformities occurring between the Grandeur and the overlying Meade Peak and between the Franson and the Retort phosphatic shale (fig. 3). In some areas, the Franson is overlain by marine sandstones (Peterson, 1980).

Although there is general agreement regarding the unconformable sequence boundaries, particularly the one underlying the Meade Peak, discrepancies arise in interpreting cherts and carbonates within eustatically-controlled sequences and the placement of maximum flooding surfaces. Such discrepancies are due in part to higher-order (shorter-term) sea-level fluctuations.

McKelvey and others (1959) interpreted the stratigraphic sequence from the upper part of the Grandeur to the lower part of the Rex Chert in southeastern Idaho as representing one nearly complete cycle of marine transgression and regression with the central mudstone-rich units of the Meade Peak representing deepest water conditions and overlying carbonate rocks (below the base of the Rex Chert) representing a return to shallow-water conditions. They interpreted the upper Rex Chert and overlying cherty phosphorites as representing a second cycle of transgression and regression. Sheldon (1963) recognized two transgressive-regressive cycles in the Permian rocks of western Wyoming. In the Lakeridge core (section 102 of his report), he interpreted the Meade Peak, Rex Chert, lower Shedhorn Sandstone, and lower Franson units as belonging to the lower cycle with the upper Franson, Retort, Tosi, and Ervay, extending to the upper Permian boundary as comprising the upper cycle. Sheldon did not recognize a separate eustatic cycle within the Rex Chert as did McKelvey and others (1959).

Hendrix and Byers (2000), working in the Uinta Mountains of Utah, interpreted the Meade Peak in terms of sequence stratigraphic models. They suggested the Meade Peak represents transgressive and highstand tracts and placed the surface of maximum flooding within the middle of the unit. They interpreted the entire Franson Member as a

regressive sequence leading to subaerial exposure. Hiatt (1997) placed the maximum flooding surface at the boundary between the Meade Peak and the overlying Rex Chert. Whalen (1996), working in Utah and western Wyoming, while acknowledging higher-order eustatic fluctuations, interpreted the entire Meade Peak Member as representing an overall transgressive system tract with Franson carbonates recording highstand conditions punctuated by several shoaling-upward cycles.

Lakeridge Core

The Lakeridge core was obtained from General Petroleum's Lakeridge No. 43-19-G well, drilled in Sublette County, WY (NW ¼ Section 19; T. 29 N., R. 114 W.). Murata and others (1972; p. D107 and Table 2) indicated that the 8 to 13-cm nominal diameter core was obtained from a depth interval of approximately 4,340 to 4,420 m. The core encompasses the stratigraphic interval from the upper Grandeur Member of the Park City Formation through the lower portion of the Ervay Member of the Park City Formation, including two intertonguing units of the Phosphoria Formation. This core thus represents a nearly complete and unweathered profile through the middle and late Permian strata of western Wyoming. The Lakeridge core is stored in the U.S. Geological Survey warehouse in Menlo Park, CA.

The core was described in detail by Sheldon (1963; p. 241-245 and Plate 6). Our generalized interpretation of lithofacies in the Lakeridge core is illustrated in figure 3. Lithologic classification of sample intervals is based on major-element concentrations measured as part of this study, using the following ordered criteria: phosphorite > 5% P₂O₅; sandy carbonate > 25%(CaO + MgO) and SiO₂ > 40%; carbonate > 25% (CaO + MgO); mudstone > 5% Al₂O₃; chert > 50% SiO₂, except where lithology is clearly sandstone; then, sandstone > 50% SiO₂ and < 25%(CaO + MgO); carbonatic sandstone > 50% SiO₂ and > 25%(CaO + MgO). The relatively low P₂O₅ and SiO₂ thresholds for phosphorite and chert are used to account for the samples being composites (see methods section), which may include phosphorites or cherts interbedded with other rock types. The geochemical-based classification agrees well with characterizations based solely on visual examination.

Previous Studies of the Lakeridge Core

Murata and others (1972) investigated variations in the Ca – Mg contents (via X-ray diffraction) and carbon and oxygen isotope compositions of selected carbonate beds from the Lakeridge core and from other sections in the western phosphate field. They found that 75% of the Park City dolomites had a CaCO₃ content of 50 mole percent while 50% of the Phosphoria dolomites had a somewhat greater CaCO₃ content, 51 to 54 mole percent. Assuming an initial calcium content of Ca₅₂₋₆₀, analogous to modern dolomites forming in tidal flats in the Persian Gulf, they concluded that the more permeable Park City carbonates provided for more complete recrystallization to the stable Ca₅₀ end Member through interactions with migrating fluids relative to the muddier and less permeable Phosphoria units. They found an average of only 1% MgCO₃ in the limestones they analyzed throughout the western Phosphate field. The lightest $\delta^{13}\text{C}_{\text{PDB}}$ values (-2.7 to -11.6 per mil) occurred in dolomites from the Phosphoria, which they attributed to bicarbonate input from degradation of organic matter and dolomitization during early diagenesis. Values of $\delta^{13}\text{C}_{\text{PDB}}$ in Park City dolomites were considerably heavier, up to +4.2 per mil in an eastern section, suggesting that these dolomites formed in near-shore environments, possibly in tidal flats. Plots of $\delta^{13}\text{C}$ versus $\delta^{18}\text{O}$ values for all samples indicated deposition under marine conditions. However, relatively light $\delta^{18}\text{O}$ values for dolomites from the Shedhorn Sandstone and the Ervay Member of the Park City Formation were interpreted as representing insipient incursion of fresh water into Ervay sediments, again suggesting near-shore conditions (Murata and others, 1972).

Medrano and Piper (1995) analyzed 65 discrete samples from throughout the Lakeridge core for a suite of major and minor elements. Assuming aluminum to be entirely of terrigenous origin and assuming a constant composition for each of the major rock components (terrigenous detritus, apatite, calcite, dolomite, biogenic silica, and organic matter), they developed proportionality calculations to determine the relative amount of each component present based on major-oxide concentrations. Inter-element ratios were then used to apportion minor and trace elements to terrigenous or marine fractions (Medrano and Piper, 1995). A summary of their analytical results is presented in table 1a. Previously unreported selenium concentrations for these samples are provided in

table 1b. The geochemical study by Medrano and Piper (1995) did not include the Grandeur Member underlying the Meade Peak.

These earlier studies provided an increased understanding of elemental associations and emphasized the importance of organic-matter deposition and degradation not only in phosphogenesis but also in the concentration of trace elements and in dolomitization. However, while these samples as a whole provide a useful record of the average conditions and the range of concentrations present in the Lakeridge core, individual samples may not accurately represent the stratigraphic interval in which they occur but rather layers that may have anonymously high or low concentrations of particular elements.

SAMPLING AND ANALYTICAL METHODS

Sample Selection and Preparation

Our goal was to obtain an unbiased, continuous, and integrated geochemical record through the Lakeridge core using thickness-weighted composite samples from intervals representing distinct lithologies. The samples should accurately reflect both the bulk chemistry within each stratigraphic interval and geochemical variations between lithologic units. In addition, the analytical results presented here include Hg, not previously analyzed, and a more complete record of As and Mn due to the lower detection limits obtained with current analytical methods.

Nearly all of the Lakeridge core is stored in labeled and oriented core boxes. The more fragmented pieces of several beds are stored in canvas bags. The total amount of bagged core is 5-10%.

The entire length of the boxed core was first cut lengthwise, maintaining the width and thickness of all the cut edges within as narrow a range as feasible. The core was then laid out from end to end in the storage warehouse and described in detail based on visual examination of the slabbed surfaces. Sixty-four sample intervals were delineated based on lithologic differences. A maximum sample interval of 3 m was used if lithology did not change over that interval.

The slabbed core edges were separated into the 100+ individual beds denoted by Sheldon (1963), washed and trimmed as needed to remove drilling mud or marker paint

present on the outer surfaces, and then crushed and powdered. Composite samples for each of the 64 chosen intervals were then prepared by mixing powders from the beds within each interval on a constant weight per length of core basis using the core lengths provided by Murata and others (1972). In addition to the 64 composite samples, 13 discrete samples from four beds were also selected for analyses, including three chert nodules, one pelletal phosphorite, one evaporate-filled vug, and matrix from subhorizons within a thick bed of Tosi Chert (bed To87).

Geochemical Analyses and Data Evaluation

Analyses of the powdered samples were conducted by XRAL Laboratories in Toronto, Ontario, Canada. The concentrations of major element oxides, excluding SiO₂, and the majority of minor and trace elements were measured by inductively coupled plasma-atomic emission spectroscopy (ICP-AES) after acid digestion using a low-temperature mixture of hydrochloric, nitric, perchloric, and hydrofluoric acids. Major element oxides as well as Ba, Cr, Nb, Y, and Zr were also analyzed by ICP-AES via a high-solids nebulizer following fusion with lithium metaborate in a graphite crucible. Fluorine concentrations were determined by ion-selective electrode analysis after subsamples were fused with sodium hydroxide potassium nitrate and then dissolved in dilute nitric acid. Arsenic, Sb, Se, and Tl were analyzed via hydride generation atomic absorption spectrometry (HG-AAS) following multi-step digestion with heated acid mixtures. Arsenic was also analyzed via ICP-AES. Total carbon and sulfur were determined as CO₂ and SO₂ using infrared detectors on combusted samples. Carbonate carbon was determined via coulometric titration of monoethanolamine-sorbed CO₂ evolved from the sample with hot perchloric acid. Organic carbon was calculated as the difference between total and carbonate carbon. Mercury was determined by cold vapor-AAS, following sample digestion with a mixture of sulfuric and nitric acids and potassium permanganate and peroxydisulfate. Excess potassium permanganate was reduced with hydroxylamine sulfate solution and the Hg(II) was reduced with stannous chloride. Mercury vapor was then separated and measured using a LEEMAN PS200 automated mercury analyzer. Gold, Pt, and Pd concentrations were determined for a

subgroup of 42 selected samples by Bondar Clegg Mineral Laboratories using fire-assay (lead) concentration and ICP-MS analytical methods.

Mineral compositions were determined on selected samples by X-ray diffraction (XRD) using a Philips diffractometer with a graphite monochromator and $\text{CuK}\alpha$ radiation. Samples were run from 4 - 70° 2 θ at 40 kV, 45 mA, and 10 counts per second. Semiquantitative mineral contents were determined (table 2) and classified as major (>25%), moderate (5-25%), or minor (<5%).

In order to monitor the quality of data generated by the contract laboratory (XRAL), check samples were run at a rate of 10%. The lower limit of detection and the acceptable method limits of precision and accuracy established by XRAL are provided in table 3a.

The concentrations of major oxides (excluding MnO and SiO₂) and Ba, Cr, Nb, and Y determined by the two ICP-AES techniques show excellent agreement as do the As concentrations determined by ICP-AES with acid digestion and HG-AAS techniques (table 3b). The analytical agreement between the ICP-AES techniques could not be evaluated for MnO because its concentration was below the detection limit of the lithium metaborate fusion method for most samples. SiO₂ was only analyzed by the lithium metaborate method. Correlation coefficients for the concentrations of each analyte determined by the two different methods exceeded 0.98, except for Ba (0.78), Cr (0.97), and Ti (0.97). The relatively poor agreement between Ba analyses is likely due to the low acid solubility of barite. This is supported by the consistently lower values obtained by the acid-digestion method, which averaged 88% of the concentrations reported via the lithium metaborate method.

Concentrations determined by the ICP-AES lithium metaborate fusion method are used for Ba and all major elements excluding C, F, Mn, and S (table 4). Sums for major-element oxides in all samples average 97.4% unless S (as S rather than SO₃) is included, in which case the average is 98.9%. Sulfur, as sulfide, organosulfur associated with organic matter, and sulfate in evaporative minerals and substituting for phosphate in apatite, is thus a more important sedimentary constituent than it would be for organic- and apatite-poor shales, cherts, and carbonates. A value of > 101% was obtained by using SO₃. The ICP-AES acid-digestion method values are used for Cr, Nb, and Y

because that method provides lower detection limits for these elements and is the method used for most of the remaining suite of trace elements (table 5). No values above method detection limits were obtained for Au, Bi, U, Ta, or Sn. Only one sample contained a quantifiable concentration of Th, and less than half the samples analyzed contained quantifiable concentrations of Ag, Be, Cd, Co, Eu, Ho, and Sb. Rare earth element (REE) concentrations are provided in table 6 and Au, Pt, and Pd concentrations for select samples are provided in table 7.

RESULTS AND DISCUSSION

Calculation of Normative Sedimentary Components

Previous geochemical studies of the Phosphoria Formation (Medrano and Piper, 1995; Piper and others, 2000) used end-member stoichiometries (Piper and Isaacs, 1995) to model the relative input of terrigenous and marine sediment components. These models begin with the assumption that all of the Al_2O_3 present is derived from terrigenous sources. The normalized composition of the terrigenous detrital fraction can then be determined based on the graphical relationship between Al_2O_3 and those major and minor elements that show good correlation or strong minima or maxima lines when plotted against Al_2O_3 (table 8; fig. 4). A strong correlation between element or element-oxide concentrations indicates that the two elements or oxides are almost entirely contained in a single component (e.g., the relationship between Al_2O_3 and Fe_2O_3 , K_2O , TiO_2). A well-defined minima line that extends to the origin indicates that one element is largely present in one component and that the second element is an important part of that same component but also occurs in significant concentrations in other components (e.g., Na_2O , SiO_2). The minima line then represents the elemental ratio within the shared component while the scatter above the line represents the element content in other components.

The proportion of terrigenous detritus present in each sample may be estimated assuming a constant detrital Al_2O_3 content. Extrapolation of the maxima line in the plot of CaO versus Al_2O_3 (figure 4) to near zero CaO (i.e., no calcite, dolomite, or apatite) gives an Al_2O_3 content of 15.1%, essentially the same as the world shale average (WSA) value (Turekian and Wedepohl, 1961; table 7). A similar value (~15.2%) was obtained from

Lakeridge core data used by Medrano and Piper (1995). The y-intercept of the CaO versus Al₂O₃ maxima line is 37% CaO, intermediate between the CaO content of dolomite (30.4%) and calcite (56.0%), though closer to the value for dolomite. A higher terrigenous detrital Al₂O₃ content for the Meade Peak (16.6%) was determined using the maxima line from a plot of CaO versus Al₂O₃, but shifting it to intercept the y-axis at 55.5%, the approximate CaO content in both calcite and apatite (Piper, 1999; Piper and others, 2000). However, those calculations were based on samples from the Enoch Valley mine in southeastern Idaho, where dolomite is less prominent (e.g., average MgO contents in Meade Peak rocks = 2.4% vs 6.5% in the Lakeridge). The lower Al₂O₃ content for the Lakeridge section as determined from the CaO:Al₂O₃ plot appears justified in view of the higher dolomite content and the resulting average component sum of nearly 100%. Indeed, the plot suggests that even lower values may be appropriate for units other than the Meade Peak and Franson. However, a constant terrigenous Al₂O₃ content was assumed for the entire Lakeridge core given the low number of samples analyzed for the other individual units. A constant detrital Al₂O₃ content is clearly not warranted for reworked beds (e.g., sandstones), which must be considered apart from the normative model.

Changes in slopes in major-element oxide:alumina plots, particularly in the Fe₂O₃ and K₂O plots (fig. 4), indicate shifts in the terrigenous detrital composition. Such variations appear to correspond to sequence intervals, with the Meade Peak and Franson samples – lying within one unconformity-bounded sequence - typically plotting along the same line. The TiO₂ versus alumina plot shows no discernable change in slope. Variations in elemental ratios across formation boundaries are discussed in a subsequent section.

The normative fractions of marine components are calculated using idealized compositions and the concentration of a diagnostic major-element oxide corrected for its incorporation in the detrital fraction [e.g., dolomite = (MgO – 0.07 x Al₂O₃) x 4.57]. The organic-matter fraction is calculated assuming a carbon content of 65.2% in organic residues, based on measured C contents of kerogen in the Phosphoria in western Wyoming (Powell and others, 1975). Calculation of calcite fractions requires corrections for incorporation of CaO in dolomite and apatite as well as the detrital fraction. The

formulas used to calculate these are provided in table 10; the resulting major component compositions for each sample are provided in table 11. The average component total is 99.95%, excluding one sample, To-87cmtx, which has an unrealistic total of 124.4%. As a secondary check on the component model, the weight percent of CO₂ was determined based on the calculated fractions of stoichiometric dolomite, calcite, and apatite and assuming a CO₂ content of 3.2% in apatite, the average measured in Phosphoria apatites by Piper and Kolodny (1986). The calculated CO₂ contents agree well with measured CO₂ contents, with an average difference of 0.06%. However, the calculated CO₂ content of one sample, F60, is nearly twice the measured CO₂ content. Sheldon (1963) noted and we observed that this sample contains large amounts of anhydrite which is not accounted for in the modeled components. Therefore, the calcite content (27.3%) calculated as a function of measured CaO (22.1%) is too high, as is the calculated CO₂ content. The measured and calculated CO₂ may be brought into agreement when the calcite content is 3.9%. The residual CaO (13.1%) is equivalent to an anhydrite content of 31.8%. This value is consistent with XRD results for this sample, which indicate that anhydrite is the major component (table 2). The component total for this sample, counting anhydrite, is 99.7%. The average difference between calculated and measured CO₂ values, excluding this sample and To87c-mtx, is 0.22%, the regression coefficient determined for calculated and measured CO₂ values is 0.997, and the average component sum is 100.05%. The near-ideal component totals and the close agreement between calculated and measured CO₂ contents indicate that the component model closely approximates the actual sample compositions of most samples. Obvious exceptions are the quartz-rich sand layers in the Shedhorn Sandstone beds, which are terrigenous but would be calculated as biogenic silica. These are easily identified based on major-element oxide ratios as discussed below. Figure 5 shows how the six sediment components, calculated from major-element-oxide concentrations, vary throughout the Lakeridge core.

Elemental Partitioning

Factor analysis is concerned with the inter-object relationships in a data set that are needed to place those objects (elements in this case) into common groups. These groups or factors are interpreted as representing particular minerals or sediment fractions

based on XRD mineralogy, element correlations, and our knowledge of the rock system in question. The resulting loadings or scores associated with a given factor represent the contribution of a particular element to the composition of that factor. A high factor loading for a given element is thus assumed to reflect a close association of that element with the corresponding mineral or sediment fraction.

In this study, iterated principle component analysis of log-normalized data was used to partition minor and trace elements among the major sedimentary fractions. Only those elements that were detected in at least 67% of all samples were used in the analyses; the log values of one-half the detection limits were used for elements that were not detected in a given sample. The number of factors was determined as the minimum number needed to express at least 75% of the original variance in the data set. Factor loadings were derived from Varimax orthogonal rotations of principal component eigenvectors were made using StatView™ software. Communalities, which represent the total proportion of variance for a given element that is accounted for by all of the factors, were >0.85 except for Cu, Hg, and Pb. The resulting table of factor loadings (table 12) shows that five factors account for over 80% of the variability inherent in the dataset. Al₂O₃ is strongly associated with factor two (i.e. loading of 0.95). Other analytes having a strong loading (>0.40) on this “terrigenous detrital factor” include Fe₂O₃, Na₂O, K₂O, TiO₂, S, As, Ba, Li, Ni, V, and Ce. Many of the same oxides and elements, with the exception of S, As, Ni, and V, were found to be strongly associated with terrigenous detrital material in the Monterey Formation (Piper and Isaacs, 1995) and the Meade Peak Member of the Phosphoria Formation (Piper, 1999; Piper and others, 2000). The high loading of S in the detrital factor is driven by the Park City samples as principal component analyses of these samples alone also shows the same association while analyses of Meade Peak samples shows S to be largely associated with organic carbon. This may be due to the relatively small amount of organic matter and apatite in the Park City units (table 11) and the increased importance of detrital barite to the total sulfur content. The other analytes are strongly associated with terrigenous detritus (Al₂O₃) using either subset of data. Although Ce has a high loading on factor two, it is more strongly associated with factor one, which represents apatite based on the high factor scores of P₂O₅ and F. La and Nd are also strongly associated with factor one.

As, Ni, and V are also strongly associated with factor five as are organic carbon, Cr, Cu, Hg, Mo, Se, and Zn. With the exception of As and Hg, the organic-rich Meade Peak and Retort Members contain, on average, more than twice the concentration of these elements than do the other units (e.g., the Park City units). Molybdenum, Mo, Se, V, and Zn show greater than 10-fold enrichment in these units relative. Piper (1994; 1999; 2001) showed that ratios of Cu:Zn, and Cu:Mo in the Meade Peak Member, adjusted for a terrigenous contribution, resemble their ratios in modern plankton, suggesting that these elements are largely biogenic. The same relationships are found in the more trace-element-enriched Lakeridge core samples (fig 6). Although such ratios and supporting evidence (e.g., seawater profiles) indicate their biological origin, these elements may currently reside in one or more authigenic phases, analogous to P_2O_5 in apatite. Plots of Mo, Se, and V versus TOC indicate some degree of association with organic matter. However, sharp maxima in plots of these same elements versus S ratios imply a stronger association with inorganic S-rich phases (fig 7).

Principal component analysis indicates that factor three is characterized by CaO and Sr, suggesting Sr substitution in either calcite or apatite. Barium also has a moderate (0.37) loading on factor three. Factor four is largely characterized by MgO and carbonate carbon, indicating dolomite. Factor six is characterized by MnO and Pb. This factor is heavily influenced by a single sample, To87c-mtx, consisting of matrix that had been surrounding chert nodules in the To87 bed of the Tosi Chert Member. The number of factors needed to express >75% of the sample variability is five and Mn is strongly loaded on the MgO – carbonate C factor if this one sample is excluded.

The To87c-mtx sample, from near the top of the Lakeridge core, has 20 times more As, 7.4 times more Pb, 2.3 times more Co, and nearly 2 times more MnO than any other sample as well as the highest Na_2O and Ba contents, the fourth highest Zn, and the fifth highest Fe content of any sample. Enrichment of Fe, Mn, As, Pb, and Zn in marine sediments can be the result of hydrothermal activity (Bostrom and others, 1969; Cronan, 1976; Feely and others, 1994) and colloidal-sized hydrothermal plume particles may be transmitted significant distances from vent sources (Dymond and Roth, 1988; Feely and others, 1996). Enrichment of Co may be the result of scavenging of Co from seawater by hydrothermal plume particles (Von Damm and others, 1985). Elemental enrichments

noted in the To87c-mtx sample may signal the proximity of an island arc off the late Permian coast. Sheldon (1963; p. 145-146) identified volcanic material in the upper Lakeridge core (sample Rt-77, Retort Member). The interval between Rt-77 and To87 is approximately 12.5 m, suggesting intermittent volcanism may have occurred for perhaps millions of years. However, the scarcity of volcanogenic material belies the significance of island-arc volcanism on the overall geochemistry of sediments deposited in the Phosphoria basin.

Temporal Variations in Geochemistry

Terrigenous Elements

The Phosphoria Basin is relatively unique among epicontinental basins in that the overall sedimentation rate was very low (Piper and Link, 2002) and the terrigenous sediment supply was primarily wind deposited (Carroll and others, 1998). Mixing of terrigenous sediments in such a setting would be minimal and the terrigenous geochemical signature may be expected to remain stable for long periods. Assuming that the primary source of Al_2O_3 , Fe_2O_3 , K_2O , and TiO_2 is terrigenous detritus, then any excursion or offset in ratios of these elements must be explained either by shifting terrigenous sediment sources or fractionation of terrigenous sediment by some reworking mechanism. If the terrigenous sediment was primarily wind-transported, then a shift in sediment provenance would represent either a long-term shift in atmospheric circulation patterns or a large-scale eustatic change that inundated or exposed particular sediment sources. However, shoreward regions, as represented by the Lakeridge section, are most likely to have been impacted by sediments from the north (e.g., the Shedhorn Sandstone) and, possibly, by fine particulates transported by near-surface waters from lagoon or sabhka environments to the east.

A plot of terrigenous detritus with stratigraphic position in the Lakeridge core shows intervals of maximum terrigenous sedimentation near the middle of the Meade Peak and Franson units and near the bottom of the Retort-Tosi sequence (fig 5). Average detrital element-oxide ratios typically approximate WSA values (fig 8). However, two types of offsets from the WSA “baseline” are apparent: 1) relatively short-lived, lithologically controlled excursions and 2) long-lasting offsets that cut across variable rock types. The first type of offset is most clearly typified by $\text{SiO}_2:\text{Al}_2\text{O}_3$ and $\text{TiO}_2:\text{Al}_2\text{O}_3$

ratios (fig 8). $\text{SiO}_2:\text{Al}_2\text{O}_3$ ratios approximate the WSA ratio of ~ 4 except in cherty zones, where SiO_2 is biogenically enriched, and in beds of the Shedhorn Sandstone. $\text{TiO}_2:\text{Al}_2\text{O}_3$ ratios are slightly enriched (2 –3 fold) above WSA values only in the Shedhorn Sandstone and sandy beds at the top of the Franson Member (fig. 8). Clearly, these sandstone layers and the ratio offsets reflect reworking and size fractionation and represent a modification of the terrigenous input that is not reflected in the component model. Lesser Si enrichments in the uppermost Rex and Tosi Chert Members are consistent with their gradational contacts with the overlying Shedhorn beds (Sheldon, 1963). Franson beds F64 – F74 ($\sim 48 - 54$ m above the base of the Meade Peak) are highly burrowed. These burrows are partly infilled with both calcite and quartz, which explains the offset in $\text{SiO}_2:\text{Al}_2\text{O}_3$ ratios. Biologic reworking of sediments may also have contributed to the high $\text{TiO}_2:\text{Al}_2\text{O}_3$ ratios in these beds.

$\text{Fe}_2\text{O}_3:\text{Al}_2\text{O}_3$ ratios throughout the Grandeur, Meade Peak, and Franson intervals (i.e., within the lower two eustatic cycles) average $\sim 0.30 - 0.35$, considerably less than the WSA value of 0.45 (fig. 8). The baseline in plots of $\text{Ba}:\text{Al}_2\text{O}_3$ and $\text{Sc}:\text{Al}_2\text{O}_3$ ratios with stratigraphic position closely approximates their respective WSA values. $\text{Fe}_2\text{O}_3:\text{Al}_2\text{O}_3$, $\text{Ba}:\text{Al}_2\text{O}_3$, and $\text{Sc}:\text{Al}_2\text{O}_3$ ratios all display sharp prominent offsets in the Shedhorn units and in the upper Franson, consistent with sediment reworking (including biologic reworking below the very top of the Franson). However, both the $\text{Fe}_2\text{O}_3:\text{Al}_2\text{O}_3$ and $\text{Ba}:\text{Al}_2\text{O}_3$ plots (fig 8) show additional spikes at the base of the Meade Peak (sample M12) and higher in the member, immediately below and at base of the intertonguing Rex Chert beds (samples M43-44, M45, R46, and M47 at $\sim 17-19$ m above the base of the Meade Peak). A sharp spike in the $\text{Sc}:\text{Al}_2\text{O}_3$ ratio also occurs in the basal Meade Peak. There are no concomitant spikes in either the SiO_2 or TiO_2 vs alumina ratios in these beds and all (excluding M43-44) contain very little terrigenous detritus, based on Al_2O_3 contents ($< 1.6\%$; table 4). Lower relative rates of terrigenous sedimentation would have allowed the otherwise masked background accumulation of Fe and Ba from seawater to dominate the geochemical signatures in these beds. Evidence from marine components (discussed below) indicates that the lowered terrigenous sedimentation is not the result of dilution by accelerated biogenic input. Therefore, these beds either represent relatively short-lived changes in atmospheric circulation or periods of relatively rapid sea-level rise

that would have trapped sediments near shore. Under the latter scenario, the maximum flooding surface would correspond to sample M43-44 (~17 m above the base of the Meade Peak). Another possibility is that increased water depths allowed a shoreward movement of the zone of intersection of wave base turbulence with the low-gradient ramp surface. This would have promoted sediment reworking and winnowing, suggested by bioclastic textures in some of the samples in this interval (fig. 3), and, possibly, preferential enrichment of heavy mineral grains hosting Fe, Ba, and Sc.

The base of the Meade Peak Member throughout the Phosphoria Basin is characterized by a lag deposit of phosphorite pellets, disarticulated bivalves and other bioclastic debris, and apparent carbonate and phosphate rip-up clasts from the underlying Grandeur Member of the Park City Formation. This bed (commonly referred to as the “fish-scale bed”) represents the lower sequence boundary of the Franson stratigraphic sequence. The spikes in Fe_2O_3 , Ba, and Sc versus alumina ratios in sample M-12 may, therefore, be the result of both reworking and low terrigenous-sediment input.

The second type of offset in major-oxide ratios is best typified by $\text{K}_2\text{O} / \text{Al}_2\text{O}_3$ ratios (fig. 8), which show long-lasting excursions well away from WSA values, particularly in the lowermost Grandeur Member of the Park City and in the Retort and Tosi Members of the Phosphoria (fig. 8). We interpret these offsets as representing shifts in terrigenous sediment sources, by virtue of their duration and lack of confinement to a single lithology. The offsets at the top of the Grandeur (where average $\text{K}_2\text{O} / \text{Al}_2\text{O}_3$ ratio values change from 0.41 to 0.26) and the bottom of the Retort Member (0.26 to 0.34) correspond to regional unconformable sequence boundaries (fig. 8). These contacts represent prolonged periods of erosion or non-deposition during which source beds may have changed or atmospheric circulation patterns and climate may have changed. A shift in the $\text{Fe}_2\text{O}_3:\text{Al}_2\text{O}_3$ baseline also occurs at the base of the Retort (fig. 8), further supporting a different terrigenous sediment source during deposition of the upper Phosphoria sediments. Widely fluctuating $\text{K}_2\text{O}:\text{Al}_2\text{O}_3$ values (0.06 to 0.52) are found in thin beds at the top of the Rex Chert and in the overlying Shedhorn Sandstone. The low extreme is reasonable in that fine grained, K-rich clays or micas may be preferentially removed over other aluminosilicates via winnowing and reworking of sands. The high

value at the top of the Rex Chert may represent a transitional facies in which the winnowed fines were trapped.

Marine Elements

Variations in ratios of elements that are derived from seawater by precipitation, adsorption, and biologic uptake should reflect changes in the paleoenvironment of deposition. In order to evaluate temporal variations of these elements, their measured bulk concentrations are first corrected to account for that portion occurring in the terrigenous component using the equation:

$$M = T - D \times (\% \text{ terrigenous fraction})$$

where M is the marine-derived concentration, T is the total element concentration, and $D \times (\% \text{ terrigenous fraction})$ represents the portion of the total concentration contributed by terrigenous detrital material. The concentration of the element associated with the terrigenous component, D, is assumed to equal the world shale average concentration. The total concentrations of several elements either are below detection limits or can be attributed entirely to terrigenous debris. This is particularly the case in the middle Franson and less so in the Grandeur and Ervay units.

Comparison of elements that precipitate from seawater under distinctly different redox conditions should help to constrain the Eh of bottom waters during deposition of the various units. For example, CrO_4^{-2} is the dominant form of dissolved Cr under oxic and neutral to alkaline pH conditions. Reduction of Cr(VI) and subsequent precipitation of Cr(III) as $\text{Cr}(\text{OH})_3$ or Cr_2O_3 occurs under moderately reducing (denitrifying or suboxic) conditions (Eh \sim 0.5 at pH 8, T = 5 to 25°C, and seawater Cr concentrations of \sim 0.2 ppb; Emerson and others, 1979). Metal sulfides readily precipitate once sufficient HS^- is available through sulfate reduction (e.g., at \sim -0.05 Eh for Cu_2S assuming similar conditions). A plot of Cr versus Cu with stratigraphic position (fig. 9) shows that the ratios exceed the values of deep seawater throughout the lower and upper Phosphoria units. The high values in the Phosphoria are indicative of precipitation under denitrifying (suboxic) conditions, which would facilitate direct Cr precipitation from seawater but allow for Cu accumulation only via biogenic input.

Under strongly denitrifying or sulfate-reducing conditions (Eh $<$ \sim -0.04), the dominant form of V in seawater (HVO_4^{-2}) will be reduced and V will precipitate as V_2O_4

(Medrano and Piper, 1995; Piper and Isaacs, 1995). Copper should precipitate as Cu_2S only under sulfate reducing conditions. The plot of V versus Cu with stratigraphic position (fig. 9) shows that the V:Cu ratio is greater than that in modern marine plankton over the same intervals in which Cr:Cu ratios are highest. However, the V:Cu ratio only equals or exceeds the value of deep seawater (~ 10) in the basal Meade Peak and in the lower part of the Retort – Tosi units. These data suggest that low-redox conditions in bottom waters, approaching sulfate reduction, were only sustained during deposition of these particular intervals. The high V:Cu value (5.9) in the upper Franson bed (fig. 9) may be due to reworking and concentration of relatively V-rich terrigenous phases (sand, silt). V:Cr do not at any point reach the value of deep seawater and exceed the value of modern phytoplankton only in the lower and middle Meade Peak Member (fig 9). This further suggests that bottom waters may have experienced extreme suboxic to euxinic conditions ($\text{Eh} < -0.04$) only during deposition of the lower half of the Meade Peak.

Further constraints on paleoredox conditions may be obtained by comparing elements that precipitate only under sulfate-reducing conditions. Reduction of Mo(VI) as MoO_4^{2-} and precipitation of MoS_2 and ZnS from seawater occurs under moderate sulfate-reducing conditions ($\text{Eh} \approx -0.15$ to -0.18 at $\text{pH} \sim 8$ and $T = 5 - 25$ C). With few exceptions, the ratios of marine Mo versus Zn throughout the Lakeridge core (fig. 9) lie more than two orders of magnitude below the deep seawater value of ~ 20.4 and nowhere do they exceed even one-fifth the seawater value.

The lowermost beds of the Meade Peak Member appear to represent the only period of deposition in which bottom waters were denitrifying for sufficiently long periods to produce ratios of Cr:Cu, V:Cu, and V:Cr above that of marine plankton. However, the low Mo:Zn ratio suggests that sulfate-reducing conditions either did not occur in the bottom waters of the Phosphoria Basin or were so brief they left no demonstrable geochemical signature. The lower Meade Peak also contains the highest organic matter content ($> 10\%$). Given that this unit lies above a recognized sequence boundary (regional unconformity) and the basin margin setting of the Lakeridge section, these beds were likely deposited in a relatively shallow, inner-middle to inner ramp position. Under such shallow conditions, a relatively high fraction of the total organic matter raining down from the photic zone is likely to have reached the seafloor (Suess,

1980). Therefore, even moderate levels of primary production may have led to nearly complete depletion of available oxygen and nitrate during deposition of this interval.

Samples M40-42 and M43-44 (~ 15 – 17 m above the base of the Meade Peak) appear to represent an important shift in paleoenvironmental conditions during deposition of the Meade Peak Member. Marine element ratios are offset over this interval; marine Cr:Cu and V:Cu ratios decrease while total S:TOC and marine V:Cr and Mo:Zn ratios increase (fig. 9). These offsets persist throughout the overlying ~7.5 m, including the interbedded Meade Peak – Rex Chert interval (samples M43 to R50). The S:TOC ratio offset is due to an abrupt decrease in the organic matter content in the Meade Peak Member at M40-42, dropping from an average of 5.7% below this sample (n = 18) to an average of 0.4 weight percent above (n = 9; t = 3.83, df = 17; see fig. 5). Such a shift indicates a drop in primary production, assuming that accumulation is driven by primary production (Pedersen and Calvert, 1990) rather than bottom water redox conditions (Ryan and Cita, 1977; Rossignol-Strick and others, 1982). A drop in primary production would decrease oxygen demand both in the sediment and bottom waters. The calculated terrigenous debris content also drops significantly above this sample, from an average of 33.1 weight percent below and including M40-42 (n = 19) to an average of 14.3 weight percent above (n = 8; t = 3.3; df = 24). Low terrigenous sedimentation was a likely precondition for widespread colonization of sponges, whose spicules are the source of silica for the Rex Chert. Such a decrease would also amplify the constant, low-level authigenic input of elements via diffusion, adsorption, and precipitation, further contributing to the offset in marine element ratios.

We suggest these changes in sediment geochemistry within the Meade Peak were brought about by rising sea levels. A rise in sea level would be expected to have the most pronounced effect on the accumulation of organic-carbon-enriched sediments in relatively shallow, marginal areas. A 3rd-order rise in sea level of 50 – 100 m (Ross and Ross, 1995) may have more than doubled the ocean depth in such a setting. A greater water depth would promote oxidation of a substantially greater portion of organic matter during settling from surface waters (Suess, 1980). In addition, a rise in sea level and the resulting landward shift in the shoreline would have trapped sediment nearer shore, reducing terrigenous input. This is consistent with the observed decrease in the

terrigenous fraction, assuming a significant part was water transported. Periods of low terrigenous sedimentation (i.e., “condensed sections”) are typically equated with maximum flooding surfaces, which represent the period of maximum rate of sea-level rise, separating transgressive system tracts from highstand conditions.

Faunal evidence in the form of a transition from conodonts (*Mesogondolella idahoensis* to *Mesogondolella serrata*) places the boundary between the Guadalupian and Leonardian series rocks and the onset of a 3rd-order marine transgression in the lower half of the Meade Peak Member (Wardlaw and Collinson, 1986; Ross and Ross, 1995; Wardlaw and others, 1995; Hiatt, 1997). Rising sea level, resulting in flooding of terrigenous sediment sources, increased sediment transport distances, and, possibly, inundation of barriers that had previously retained sediments from alternate source areas (e.g., the Goose Egg Basin) may have modified the composition of the terrigenous component. A change in the composition of the terrigenous debris fraction that was deposited in the Phosphoria Basin is suggested by offsets in the average $\text{TiO}_2 : \text{Al}_2\text{O}_3$, and $\text{K}_2\text{O} : \text{Al}_2\text{O}_3$ ratios (apparent as a decrease in the baseline of the first ratio at ~ 7 - 8 m above the base of the Meade Peak and lower minima in the latter ratio at ~ 10 m; fig. 8). A discrete offset to lower average $\text{K}_2\text{O} : \text{Al}_2\text{O}_3$ ratios has also been identified in this part of the section (lower central waste zone of the Meade Peak Member) in other areas spanning the Phosphoria Basin (unpublished data). These changes could have taken place even in early stages of sea-level rise, given the relatively low gradient surface of the ramp margin (Liu and others, 1998). A dramatic decline in terrestrial sedimentation may have occurred only during the most rapid period of sea-level rise (i.e. maximum flooding).

Under this scenario, the offsets in the terrigenous element-oxide ratios and the decrease in dolomite content (~7-8 m above the base of the Meade Peak) likely represent the onset of a major rise in sea level. The maximum flooding surface, separating the transgressive and highstand tracts, may be represented by the sharp decrease in both terrigenous sediment and organic matter at ~17 m above the base of the Meade Peak (at sample M43-44). The high Fe_2O_3 and Ba versus alumina ratios in sample M45 (~ 18 m) would reflect minimum terrigenous sedimentation in the early highstand tract, preceding shoaling during deposition of the interbedded Rex Chert and uppermost Meade Peak layers. Shoaling in these layers is evidenced by chaotic bedding and bioclasts.

The interval of relatively rapid sea-level rise in the Ervay sequence (Retort – Ervay units) can be identified using similar lines of evidence. In this younger section, there is a sharp and significant decrease in the terrigenous component, as well as a less dramatic decrease in dolomite and a slight increase in calcite in the Tosi Chert Member at ~ 66 m above the base of the Meade Peak (sample To85; fig. 5). Similar to the Meade Peak, there are maxima in the Ba:Al₂O₃ ratio in the overlying bed (To86(0-5.5)), as well as shifts in localized average Sc:Al₂O₃ and K₂O:Al₂O₃ ratios (fig. 8). One difference between the two sequences is that these shifts occur in the Tosi Chert Member of the upper (Ervay) sequence, but below the Rex Chert in the lower (Franson) sequence. This is consistent with a study of the Ervay sequence in the Bighorn Basin by Clarke (1994), who determined that the maximum flooding surface lay above chert-rich layers in some sections.

Cerium anomalies for Lakeridge core samples were calculated using:

$$\text{Ce Anomaly (Ce}^*) = \log (3 \times \text{Ce}_{\text{Norm}} / (2 \times \text{La}_{\text{Norm}} + \text{Nd}_{\text{Norm}}))$$

where Ce_{Norm}, La_{Norm}, and Nd_{Norm} are the shale-normalized concentrations of Ce, La, and Nd (Piper, 1974). The Ce anomaly values average -0.50 for the entire core (fig. 9). They are consistently negative but approach zero within the Grandeur (e.g., sample Ws5; Ce* = -0.08) and through the lower to middle Franson (e.g., samples F62 and F64(0-5); Ce* = -0.09 and -0.06). Negative Ce anomalies are consistent with lower denitrifying waters as precipitation of insoluble cerium oxide or hydroxide would have occurred under higher redox potential (de Baar and others, 1988). Small Ce anomalies (i.e., REE relationships approaching those of world shale) in the two zones in the Grandeur and Franson units could reflect the high terrigenous debris content (>29%) in these samples. However, the Ce* values in these intervals are much closer to zero than for other intervals with much higher terrigenous contents (e.g., samples M32 and M34, which have average calculated terrigenous debris contents of 61.2 and 71.7% and Ce* values of -0.34 and -0.31, respectively). Another possible explanation for the small Ce* values is that the sediment in these intervals were deposited under higher redox (oxic to upper denitrifying)

conditions (de Baar and others, 1988; Sholkovitz and others, 1994). This is consistent with the extensive burrowing that we noted throughout the upper (Franson) interval.

Variations in Trace Element Concentrations

The Meade Peak Member of the Phosphoria Formation contains relatively high levels of various trace elements that may be of environmental concern. The chemistry of other upper Permian units has been less studied owing to their lack of economically-extractable phosphate. Previous studies of the trace elements in the Meade Peak focused on surface mining sites where rocks are almost certainly more weathered than in the Lakeridge core. Therefore, we have included plots showing variations in concentrations of six trace elements of concern (Cd, Cr, Ni, Se, V, and Zn) with stratigraphic position in the Lakeridge core (fig. 10).

These plots clearly show that the highest concentrations occur in the basal Meade Peak and that the highest concentrations represent ~10- to 1400-fold enrichment of these elements over their WSA values (table 9). High levels of Zn (500 – 1700 ppm) also occur in the uppermost Meade Peak. A slight enrichment of Cr, Ni, and Se above WSA contents occurs in the Retort Member, although the concentrations of these elements are 8 – 20 times lower than the maximum concentrations in the Meade Peak.

We attribute the high concentrations of these six elements in the basal Meade Peak Member to two factors: 1) relatively shallow waters, which allowed a large percentage of organic material from the photic zone to reach the sea floor, by escaping oxidation in the water column, and 2) a low rate of terrigenous sedimentation. A higher rate of primary production during deposition of the lower Meade Peak could certainly play a key role in accumulation of organic-rich sediments; however, we have no evidence regarding variations in primary production rates. The high organic-matter content of these sediments accounts for the high concentrations of biogenic elements (e.g., Cu, Se, Zn) from the photic zone. The low-redox levels resulting from oxidation of the accumulating organic matter allowed for precipitation of the primarily hydrogenous elements - Cr and V- from the bottom water. Their lower concentrations in the Retort Member suggests this member was deposited under more oxidizing conditions, on average. That is, redox conditions likely varied between oxic and denitrifying during deposition of both

members, but were oxic more of the time during deposition of the Retort Member than during deposition of the Meade Peak Member.

SUMMARY CONCLUSIONS

The Lakeridge core provides a nearly continuous and relatively unweathered record of late Permian sedimentation along the eastern margin of the Phosphoria Basin. We present the results of major-, minor-, and trace-element analyses of stratigraphic-thickness-weighted slab-samples collected at a maximum interval of 3 m along the entire 80+ m-length of the core. Following previous work by Medrano and Piper (1992; 1995), Piper and Issacs (1995), and Piper and others (2000), we modeled variations in rock geochemistry in terms of six major host components: terrigenous siliciclastic debris, apatite, dolomite, calcite, organic matter, and biogenic silica. Graphical and factor analyses indicate that Ba, Co, Ga, Li, and Sc are now hosted largely in the terrigenous debris and were likewise supplied by the terrigenous fraction. These analyses suggest that significant amounts of Pb, Ni, and Ce are also associated with the terrigenous sediment fraction. Arsenic, Cd, Cr, Cu, Hg, Mo, Ni, Se, V, and Zn are associated with organic carbon. However, the occurrence of several of these, especially Cr and V, are likely the result of precipitation /adsorption reactions from seawater, driven by low-redox (denitrifying or suboxic) conditions resulting from high organic-matter loading. The factor analysis also indicates that Sr substitutes for Ca in either calcite or, more likely, apatite. One sample of the Tosi Chert contains anomalously high contents of As, Co, Mn, and Pb, which we tentatively suggest were derived from incorporation of particulates from hydrothermally active areas, presumably from a volcanic arc to the west. We attribute the high Co concentrations to scavenging of seawater Co by these particulates.

Relationships among elements associated with the terrigenous or marine sediment fractions are used to investigate temporal variations in rock geochemistry. Interpretations of variations in element ratios are made assuming sediment deposition along a low-gradient, siliclastic-carbonate ramp (Burchette and Wright, 1992; Tucker and others, 1993) and within the confines of a previously recognized sequence stratigraphy framework (Peterson, 1980; Clark, 1994; Ross and Ross, 1995; Whalen, 1996; Hiatt, 1997; Hendrix and Byers, 2000). Major shifts in element ratios characteristic of

terrigenous debris that occur at sequence boundaries at the base of the Meade Peak and Retort Members of the Phosphoria Formation are attributed to changing sediment sources. Spikes in Fe, Ba, and Sc to alumina ratios that occur in the upper Retort, the upper Franson, the upper Meade Peak, and in the Shedhorn Sandstone, represent either authigenic inputs of these otherwise terrestrial elements, which become dominant during periods of extremely low terrigenous sedimentation or reworking of terrigenous sediment in shoreward facies.

Trends in element ratios characteristic of marine input reflect variations in primary productivity and redox conditions of bottom waters. Inter-element relationships in the marine fraction indicate that bottom waters of the Phosphoria Basin were predominantly denitrifying during deposition of the Ervay and Phosphoria sediments, although sulfate-reducing conditions may have existed during deposition of the lower Meade Peak sediments. Oxidic conditions during deposition of a large part of the Franson and Grandeur could not be evaluated by marine element ratios as concentrations of marine elements either were below detection limits or could be wholly attributable to terrigenous debris. However, the lack of significant marine Cr and V, as well as the near-zero values for Ce anomalies and extensive burrowing suggest that oxidic conditions were attained during deposition of these units. This would be consistent with sedimentation in a shallow, inner- to back-ramp setting. Oxidic conditions also likely occurred during part of the time of deposition of the Retort Member.

Variations in sediment facies and organic matter and trace element contents largely reflect changes in Permian sea level. Both terrestrial- and marine-element ratios appear useful in identifying the intervals representing the onset of sea-level rise and periods of maximum rates of sea-level rise (maximum flooding events). Changes in sea level likely had a much more pronounced effect in marginal areas, such as represented by the Lakeridge section, than in deeper portions of the basin. Water depths near the margins of the Phosphoria Basin may have been doubled by a 3rd-order rise in sea level of 50 – 100 m. This would have allowed for more complete oxidation of settling organic matter and likely resulted in a shift in the zone of upwelling. A relatively rapid period of sea-level rise (represented by shifts in elemental ratios above and below sample M43-44) led to significant landward shift of the shoreline and a dramatic decrease in terrigenous

sedimentation. Shoaling during late high-stand conditions (regression) is reflected by accumulation of sponge spicules (chert beds), increased sand content, chaotic bedding, and bioclastic textures. Falling sea levels may have allowed for increased organic accumulation, leading to the deposition of the uppermost Meade Peak phosphorites. This interpretation suggests that phosphogenesis can occur under lowstand, transgressive, and highstand conditions in marginal areas, assuming water depths are sufficient for upwelling to occur. Formation of phosphorite layers appears to have been most dependent on a lack of dilution by terrigenous sedimentation and carbonate shoaling.

Continued shoaling lead to deposition of the Shedhorn Sandstone, Franson carbonates, and, eventually, evaporate-rich beds in a protected, subaerial, back ramp setting (Tucker and others, 1993). A return to deeper water conditions in the uppermost Franson is suggested by marine element ratios (fig. 9) and increased sand content, signifying increased bottom water energy conditions and winnowing of sediments. This is consistent with the start of an upper transgressive-regressive cycle that Sheldon (1963) placed at the change to pale mudstone, pale dolomite, and dolomitic sandstones in the Franson (as in the pale, brownish-gray, slightly sandy dolomite of bed F74). However, the unconformable boundary between the Franson and Ervay stratigraphic sequences is evident in the sharp offsets in major element-oxide ratios, particularly that of $K_2O:Al_2O_3$ (fig. 8). The overlying Ervay sequence represents a similar evolution, although higher rates of diluting terrigenous sediment during deposition of the Retort in the Lakeridge area may have limited the accumulation of organic matter and associated trace elements to lower levels than in the Meade Peak. This is consistent with prior interpretations of a more shoreward setting for the upper Phosphoria (Murata and others, 1972).

ACKNOWLEDGEMENTS

We thank Phil Moyle for reviewing this report.

REFERENCES

- Bostrom, K., Peterson, M.N.A., Joensuu, O. and Fisher, D.E., 1969, Aluminium-ppor ferromanganooan sediments on active oceanic ridges: *Journal of Geophysical Research*, v. 74, p. 3261-3270.
- Boyle, E.A., Sclater, F.R. and Edmond, J.M., 1976, On the marine geochemistry of cadmium: *Nature*, v. 263, p. 42-44.

- Boyle, E.A., Sclater, F.R. and Edmond, J.M., 1977, The distribution of dissolved copper in the Pacific: *Earth and Planetary Science Letters*, v. 37, p. 38-54.
- Bruland, K.W. and Franks, R.P., 1983, Mn, Ni, Cu, Zn, and Cd in the western North Atlantic, *in* Wong, C.S., Boyle, E., Bruland, K.W., Burton, J.D., and Goldberg, E.D., eds., *Trace metals in sea water*: Plenum Press, New York, p. 395-414.
- Brumsack, H.J., 1986, The inorganic geochemistry of Cretaceous black shales (DSDP Leg 41) in comparison to modern upwelling sediments from the Gulf of California, *in* Summerhayes, C.P. and Shackleton, N.J., eds., *North Atlantic paleoceanography*, Special Publication, Geological Society of London, p. 447-462.
- Burchette, T.P. and Wright, V.P., 1992, Carbonate ramp depositional systems: *Sedimentary Geology*, v. 79, p. 3-57.
- Carroll, A.R., Stephens, N.P., Hendrix, M.S. and Glenn, C.R., 1998, Eolian-derived siltstone in the Upper Permian Phosphoria Formation; implications for marine upwelling: *Geology*, v. 26, p. 1023-1026.
- Clark, W.J., 1994, The Ervay cycle of the Permian Phosphoria and Park City formations, Bighorn Basin, Wyoming; sequence stratigraphy, facies, and porosity trends. Ph.D. Thesis, University of Colorado, Boulder, 606 pp.
- Collier, R.W., 1985, Molybdenum in the northeast Pacific Ocean: *Limnology and Oceanography*, v. 30, p. 1351-1354.
- Collier, R.W. and Edmond, J.M., 1984, The trace element chemistry of marine biogenic particulate matter: *Progress in Oceanography*, v. 13, p. 113-119.
- Cronan, D.S., 1976, Manganese nodules and other ferromanganese oxide deposits: *Chemical Oceanography*, v. 5, p. 217-263.
- de Baar, H.J.W., German, C.R., Elderfield, H. and van Gaans, P., 1988, Rare earth element distribution in anoxic waters of the Cariaco Tranch: *Geochimica et Cosmochimica Acta*, v. 52, p. 1203-1219.
- Dymond, J. and Roth, S., 1988, Plume dispersed hydrothermal particles; a time-series record of settling flux from the Endeavour Ridge using moored sensors: *Geochimica et Cosmochimica Acta*, v. 52, p. 2525-2536.
- Emerson, S.R., Cranston, R.E. and Liss, P.S., 1979, Redox species in a reducing fjord - equilibrium and kinetic observations: *Deep-Sea Research*, v. 25, p. 859-878.
- Feely, R.A., Baker, E.T., Marumo, K., Urabe, T., Ishibashi, J., Gendron, J., Lebon, G.T. and Okamura, K., 1996, Hydrothermal plume particles and dissolved phosphate over the superfast-spreading southern East Pacific Rise: *Geochimica et Cosmochimica Acta*, v. 60, p. 2297-2323.
- Feely, R.A., Massoth, G.J., Trefry, J.H., Baker, E.T., Paulson, A.J. and Lebon, G.T., 1994, Composition and sedimentation of hydrothermal plume particles from North Cleft Segment, Juan de Fuca Ridge: *Journal of Geophysical Research*, B, Solid Earth and Planets, v. 99, p. 4985-5006.
- Gulbrandsen, R.A. and Krier, D.J., 1980, Large and rich phosphorus resources in the Phosphoria Formation in the Soda Springs area, southeastern Idaho: *U.S. Geological Survey Bulletin B-1496*, 25 p.
- Hendrix, M.S. and Byers, C.W., 2000, Stratigraphy and sedimentology of Permian strata, Uinta Mountains, Utah; allostratigraphic controls on the accumulation of economic phosphate, *in* Glenn, C.R., Prevot-Lucas, L., and Lucas, J., eds., *Marine authigenesis*;

- from global to microbial: Special Publication, v. 66, Society for Sedimentary Geology (SEPM), Tulsa, p. 349-367.
- Hiatt, E.E., 1997, A paleoceanographic model for oceanic upwelling in a late Paleozoic epicontinental sea; a chemostratigraphic analysis of the Permian Phosphoria Formation: Ph.D. Thesis, University of Colorado, Boulder, 294 pp.
- Inden, R.F. and Coalson, E.B., 1996, Phosphoria Formation (Permian) cycles in Bighorn Basin, Wyoming, with emphasis on the Ervay Member, *in* Longman, M.W. and Sonnenfeld, M.D., eds., Paleozoic systems of the Rocky Mountain region: Society for Sedimentary Geology (SEPM), Denver, p. 379-404.
- Liu, K., Liang, T.C.K., Paterson, L. and Kendall, C.G.S.C., 1998, Computer simulation of the influence of basin physiography on condensed section deposition and maximum flooding: *Sedimentary Geology*, v. 122, p. 181-191.
- Martin, J.H. and Knauer, G.A., 1973, The elemental composition of plankton: *Geochimica et Cosmochimica Acta*, v. 37, p. 1639-1653.
- Maughan, E.K., 1984, Geological setting and some geochemistry of petroleum source rocks in the Permian Phosphoria Formation, *in* Woodward, J., Meissner, F.F., and Clayton, J.L., eds., Hydrocarbon source rocks of the Greater Rocky Mountain region: Rocky Mt. Association of Geologists, Denver, p. 281-294.
- Maughan, E.K., 1994, Phosphoria Formation (Permian) and its resource significance in the Western Interior, U.S.A., *in* Embry, A.F., Beauchamp, B., and Glass, D.J., eds., Pangea; global environments and resources: Memoir 17, Canadian Society of Petroleum Geologists, Calgary, p. 479-495.
- McKelvey, V.E., Williams, J.S., Sheldon, R.P., Cressman, E.R., Cheney, T.M. and Swanson, R.W., 1959, The Phosphoria, Park City and Shedhorn Formations in the western phosphate field: U.S. Geological Survey Professional Paper 313-A, 47 p.
- Medrano, M.D. and Piper, D.Z., 1992, A normative-calculation procedure used to determine mineral abundances in rocks from the Montpelier Canyon section of the Phosphoria Formation, Idaho; a tool in deciphering the minor-element geochemistry of sedimentary rocks: U. S. Geological Survey, Bulletin 2023-A, 28 p.
- Medrano, M.D. and Piper, D.Z., 1995, Partitioning of minor elements and major-element oxides between rock components and calculation of the marine derived fraction of the minor elements in rocks of the Phosphoria Formation, Idaho and Wyoming: U.S. Geological Survey Open File Report 95-0270, 79 p.
- Murata, K.J., Friedman, I. and Gulbrandsen, R.A., 1972, Geochemistry of carbonate rocks in Phosphoria and related formations of the western Phosphate Field: U.S. Geological Survey, Professional Paper 800-D, p. D103-110.
- Pedersen, T.F. and Calvert, S.E., 1990, Anoxia vs productivity; what controls the formation of organic-carbon-rich sediments and sedimentary rocks?: *AAPG Bulletin*, v. 74, p. 454-466.
- Peterson, J.A., 1980, Depositional history and petroleum geology of the Permian Phosphoria, Park City, and Shedhorn formations, Wyoming and southeastern Idaho: U.S. Geological Survey Open File Report 80-667, 42 p.
- Piper, D.Z., 1974, Rare earth elements in the sedimentary cycle - a summary: *Chemical Geology*, v. 14, p. 285-304.
- Piper, D.Z., 1994, Seawater as the source of minor elements in black shales, phosphorites and other sedimentary rocks: *Chemical Geology*, v. 114, p. 95-114.

- Piper, D.Z., 1999, Trace elements and major-element oxides in the Phosphoria Formation at Enoch Valley, Idaho; Permian sources and current reactivities: U.S. Geological Survey Open File Report 99-0163, 66 p.
- Piper, D.Z., 2001, Marine chemistry of the Permian Phosphoria Formation and basin, Southeast Idaho: *Economic Geology*, v. 96, p. 599-620.
- Piper, D.Z. and Isaacs, C.M., 1995, Geochemistry of minor elements in the Monterey Formation, California; seawater chemistry of deposition. U.S. Geological Survey Professional Paper P-1566, 41 p.
- Piper, D.Z. and Kolodny, Y., 1986, Stable isotopic composition of a marine phosphate deposit: Deep-Sea Research. Part A: Oceanographic Research Papers, v. 34, p. 897-911.
- Piper, D.Z. and Link, P.K., 2002, An upwelling model for the Phosphoria Sea - a Permian, ocean-margin basin in the northwest United States. *American Association of Petroleum Geologists Bulletin*, v. 86, p. 1217-1235.
- Piper, D.Z., Skorupa, J.P., Presser, T.S., Hardy, M.A., Hamilton, S.J., Huebner, M. and Gulbrandsen, R.A., 2000, The Phosphoria Formation at the Hot Springs Mine - a source of selenium and other trace elements to ground water, surface water vegetation and biota: U.S. Geological Survey Open File Report 00-050, 73 p.
- Powell, T.G., Cook, P.J. and McKirdy, D.M., 1975, Organic geochemistry of phosphorites; relevance to petroleum genesis: *American Association of Petroleum Geologists Bulletin*, v. 59, p. 618-632.
- Ross, C.A. and Ross, J.R.P., 1995, Permian sequence stratigraphy, *in* Scholle, P.A., Peryt, T.M., and Ulmer-Scholle, D.S., eds., *The Permian of northern Pangea; Volume I, Paleogeography, paleoclimates, stratigraphy*: Springer-Verlag, Berlin, p. 98-123.
- Rossignol-Strick, M., Nesteroff, W., Olive, P. and Vergnaud-Grazzini, C., 1982, After the deluge: Mediterranean stagnation and sapropel formation: *Nature*, v. 295, p. 105-110.
- Ryan, W.B.F. and Cita, M.B., 1977, Ignorance concerning episodes of ocean-wide stagnation: *Marine Geology*, v. 23, p. 197-215.
- Sheldon, R.P., 1963, Physical stratigraphy and mineral resources of Permian rocks in western Wyoming: U.S. Geological Survey Professional Paper 313-B, p. 49-273.
- Sholkovitz, E.R., Landing, W.M. and Lewis, B.L., 1994, Ocean particle chemistry: the fractionation of rare earth elements between suspended particles and seawater: *Geochimica et Cosmochimica Acta*, v. 58, p. 1567-1579.
- Suess, E., 1980, Particulate organic carbon flux in the oceans; surface productivity and oxygen utilization: *Nature*, v. 288, p. 260-263.
- Tisoncik, D.D., 1984, Regional lithostratigraphy of the Phosphoria Formation in the Overthrust Belt of Wyoming, Utah and Idaho, *in* Woodward, J., Meissner, F.F., and Clayton, J.L., *Hydrocarbon source rocks of the Greater Rocky Mountain region, Rocky Mt. Association of Geologists*, Denver, p. 295-320.
- Tucker, M.E., Calvet, F. and Hunt, D., 1993, Sequence stratigraphy of carbonate ramps; systems tracts, models and application to the Muschelkalk carbonate platforms of eastern Spain, *in* Posamentier, H.W., Summerhayes, C.P., Haq, B.U., and Allen, G.P., eds., *Sequence stratigraphy and facies associations: Special Publication of the International Association of Sedimentologists*, v. 18, p. 397-415.

- Turekian, K.K. and Wedepohl, K.H., 1961, Distribution of the elements in some major units of the Earth's crust: Geological Society of America Bulletin, v. 72, p. 175-191.
- Vine, J.D. and Tourtelot, E.B., 1970, Geochemistry of black shale deposits; a summary report: Economic Geology and the Bulletin of the Society of Economic Geologists, v. 65, p. 253-272.
- Von Damm, K.I., Edmond, J.M., Grant, B., Measures, C.J., Walden, B. and Weiss, R.F., 1985, Chemistry of submarine hydrothermal solutions at 21°N, East Pacific Rise: Geochimica et Cosmochimica Acta, v. 49, p. 2197-2220.
- Wardlaw, B.R. and Collinson, J.W., 1986, Paleontology and deposition of the Phosphoria Formation, *in* Boyd, D.W. and Lillegraven, J.A., eds., Western phosphate deposits, Contributions to Geology, v. 24, University of Wyoming, Laramie, p. 107-142.
- Wardlaw, B.R., Snyder, W.S., Spinosa, C. and Gallegos, D.M., 1995, Permian of the Western United States, *in* P.A. Scholle, T.M. Peryt and D.S. Ulmer-Scholle, eds., The Permian of northern Pangea; Volume 2, Sedimentary basins and economic resources: Springer-Verlag, Berlin, p. 23-40.
- Wedepohl, K.H., 1969-78, Handbook of Geochemistry: Springer-Verlag, Berlin, 4 volumes.
- Whalen, M.T., 1996, Facies architecture of the Permian Park City Formation, Utah and Wyoming; implications for the paleogeography and oceanographic setting of western Pangea, *in* Longman, M.W. and Sonnenfeld, M.D., Paleozoic systems of the Rocky Mountain region: Society for Sedimentary Geology (SEPM), Denver, p. 355-378.

Table 1a. Summary of Lakeridge core analytical data from Medrano and Piper (1995). Samples from the Grandeur Member of the Park City Formation were not analyzed. Major element oxides and F in wt. %; all others in mg kg⁻¹.

Analyte	Ervey Member, Park City Fm and Upper Shedhorn Sandstone (n = 5)			Retort Phosphatic Shale and Tosi Chert Members, Phosphoria Fm (n = 8)			Franson Member, Park City Fm and Lower Shedhorn Sandstone (n = 15)			Meade Peak and Rex Chert Members, Phosphoria Fm (n=36)		
	Min	Avg	Max	Min	Avg	Max	Min	Avg	Max	Min	Avg	Max
Al ₂ O ₃	0.45	0.77	0.98	1.29	3.33	7.75	0.01	2.48	16.6	0.43	5.50	12.5
CaO	7.84	22.6	30.8	4.90	18.4	39.2	3.64	24.5	40.6	2.38	23.4	47.6
CO ₂	4.12	25.5	40.4	4.02	12.0	23.6	4.70	27.3	43.9	0.46	8.74	39.7
F	0.10	0.30	0.46	0.17	0.82	2.8	0.04	0.31	0.62	0.06	1.38	3.70
Fe ₂ O ₃	1.60	2.29	3.33	2.47	4.37	7.25	0.45	3.07	7.25	0.62	3.36	10.3
K ₂ O	0.16	0.25	0.35	0.49	1.12	2.76	0.01	0.77	5.64	0.12	1.61	3.72
MgO	2.16	12.22	23.2	2.16	5.10	9.63	0.58	12.4	21.6	0.13	4.02	19.9
MnO	0.03	0.08	0.11	0.01	0.04	0.06	0.02	0.03	0.05	0.01	0.02	0.04
Na ₂ O	0.27	0.33	0.38	0.36	0.75	1.49	0.07	0.68	1.75	0.46	1.29	2.97
P ₂ O ₅	0.85	2.59	4.12	1.28	6.90	22.7	0.02	2.16	5.95	0.30	12.4	34.4
SiO ₂	44.0	610	79	36.6	45.0	51	7.20	24.6	490	12.6	38.1	63
SO ₃	0.12	0.45	0.90	1.40	4.12	9.74	0.32	2.92	13.0	0.42	7.28	24.5
TiO ₂	0.00	0.01	0.02	0.02	0.06	0.15	0.0	0.1	0.5	0.00	0.12	0.33
Ba	16.0	30.2	48	62	93	150	10.0	46.3	170	23.0	140	290
Cd	1.0	1.0	1.0	1.0	2.8	8.0	1.0	1.1	2.0	1.0	91	590
Co	3.0	3.5	4.0	4.0	4.8	6.0	2.0	5.1	20.0	0.5	5.3	10.0
Cr	129	174	240	180	380	670	10	142	380	110	1280	5500
Cu	22	35.6	57	42.0	59	83	7.0	48.7	130	16.0	103	480
Ga	2.0	2.0	2.0	2.0	4.3	8	2.0	3.4	17	2.0	7.8	29.0
Li	8.0	14.0	20	18.0	33.4	50	1.0	15.1	110	4.0	26.4	79
Mo	5.0	8.4	14	10.0	14.3	19	2.0	14.3	37	5.0	105.9	670
Ni	15	24.6	39	35.0	59	110	5.0	34.2	84	17.0	266	1400
Pb	2.0	10.2	20	19.0	27.3	40	2.0	4.7	14	2.0	10.7	32.0
Sc	1.0	1.8	3.0	2.0	4.3	7.0	1.0	3.1	15	1.0	8.3	14.0

Table 1a, continued

Analyte	Ervey Member, Park City Fm and Upper Shedhorn Sandstone (n = 5)			Retort Phosphatic Shale and Tosi Chert Members, Phosphoria Fm (n = 8)			Franson Member, Park City Fm and Lower Shedhorn Sandstone (n = 15)			Meade Peak and Rex Chert Members, Phosphoria Fm (n=36)		
	Min	Avg	Max	Min	Avg	Max	Min	Avg	Max	Min	Avg	Max
Se	1.3	13.8	49	1.6	7.0	16.1	0.7	10.7	42.5	1.6	82	380
Sr	74	108	140	73	339	1000	70	203	630	98	623	2000
V	18	22.0	29	22.0	59	160	6.0	35.7	180	24.0	551	3900
Y	20	51	84	16.0	98	460	5.0	45.4	170	6.0	204	900
Zn	1.0	3.4	8	4.0	195	880	1.0	16.1	83	13.0	1830	9400
La	11	33.8	55	11.0	72	340	5.3	32.4	100	8.7	153	600
Ce	5.2	14.4	25	7.7	30.5	110	5.6	20.0	690	5.3	58	260
Pr	2.1	5.6	10	1.9	10.6	50	1.2	5.4	16	1.2	20.2	86
Nd	8.4	21.9	41	8.1	41.2	200	3.8	21.4	67	4.6	77	340
Sm	1.6	4.0	7.5	1.4	6.9	33	0.8	4.0	12	0.9	12.6	59
Eu	0.3	0.9	1.4	0.3	1.5	6.8	0.2	0.8	2.7	0.2	2.7	13
Gd	1.8	4.7	8.9	1.6	8.0	38	0.7	4.5	15	0.8	15.0	76
Tb	0.2	0.7	1.3	0.2	1.2	5.6	0.1	0.7	2.3	0.1	2.2	11
Dy	1.7	4.3	7.7	1.5	7.6	35	0.6	4.3	14	0.8	14.0	68
Ho	0.4	1.0	1.7	0.3	1.7	7.7	0.1	1.0	3.2	0.2	3.3	16
Er	1.2	2.7	4.5	1.0	5.0	22	0.4	2.8	9.0	0.6	9.5	45
Tm	0.2	0.4	0.6	0.1	0.7	2.8	0.1	0.4	1.2	0.1	1.2	5
Yb	1.0	2.1	3.1	0.8	3.8	16	0.3	2.2	6.1	0.4	7.2	31

Table 1b. Previously unreported selenium concentrations for Medrano and Piper (1995) samples.

Sample	Se (mg kg⁻¹)	Sample	Se (mg kg⁻¹)
E-92C	1.3	M-48B	25.1
US-91B	3.1	M-47	5.1
E-90A	14	M-45	9
E-89A	49	M-44A	33.6
US-88C	1.5	M-42A	15.3
TO-87B	8.6	M-41	48.4
TO-86D	1.6	M-40	23.1
TO-85A	n.d.	M-39B	94
TO-84B	3.5	M-38A	163
RT-81A	4.2	M-37A	28.4
TO-78C	2	M-36B	5.5
RT-77	13.2	M-35A	31.3
RT-75A	16.1	M-34A	28.7
F-74	4	M-33A	28
F-73	4.2	M-32A	39.8
F-72B	n.d.	M-31A	21.7
F-71B	2.4	M-30A	70.7
F-70E	3	M-29A	16
F-69A	0.7	M-28A	33.7
F-68A	14.4	M-27B	6.3
F-65B	1.6	M-25	57
F-64A	2	M-24	117
LS-62A	6.8	M-23B	28.8
F-58B	2.2	M-22B	186
LS-57M	28.2	M-21A	3.7
LS-57D	42.5	M-20B	180
LS-56A	32.2	M-18	271
LS-55B	6.2	M-17	380
R-54C	1.6	M-16	308
M-53B	17.2	M-15A	318
M-52	13.2	M-14	312
R-50F	7.3	M-12B	21.5

n.d.: not detected

Table 2. X-ray diffraction mineralogy of selected samples.

Sample	Major	Moderate	Minor
To87c-mtx	Quartz	CFA, dolomite	Feldspar, mica, calcite, gypsum
F66-68	Dolomite	Quartz	Mica, pyrite, albite
F64(0-.5)	Dolomite, K-feldspar	Quartz, Plagioclase	Calcite, natrojarosite??
F62	Dolomite, quartz	Feldspar	Anhydrite, illite, gypsum
F60	Anhydrite	Quartz, dolomite, plagioclase	Calcite, kaolinite, gypsum
LS55	Dolomite, quartz	Albite	--
M51	CFA, quartz	Dolomite	--
M48	Quartz	Plagioclase, CFA, dolomite	Illite
M36-40	Quartz, dolomite	CFA	Muscovite, pyrite, goethite?
M16-18	CFA, quartz	Dolomite, goethite, muscovite	Pyrite, sphalerite, Ca,Ti-oxide?
M14-15	Quartz, dolomite	Apatite, muscovite	Calcite, albite, illite
M12	CFA, calcite	Quartz, dolomite	--
Ws-5	Quartz, dolomite	Goethite, feldspar	Mica
Ws-3	Quartz, dolomite	Anhydrite	Illite, sodalite?
Ws-1	Quartz	Dolomite, anhydrite, gypsum	Feldspar, kaolinite

Note: Estimated abundance is based on relative heights of primary peaks; Major > 25%; Moderate 5 – 25%; Minor <5%.

Table 3a. Quality control limits for the analytical techniques used in this study.

Analytical Method	DETECTION LIMITS		METHOD LIMITS			
	Analytes	Lower (mg kg ⁻¹)	Upper (wt. %)	Accuracy % Recovered ^b	Precision RSD ^c (%)	
ICP-AES using lithium metaborate fusion	Al	100	15	± 15	15	
	Si, Fe, Mg, Na	100	30			
	Ca	100	35			
	Ti, P	100	25			
	Mn, Cr	100	10			
	Ba, Nb, Sr, Y, Zr	10	10			
ICP-AES using multi-acid digestion	Al	50	50	±15	15	
	Fe	200	50			
	Mg, Ca, Na, P	50	50			
	K	100	50			
	Ti	50	25			
	Ag	2	1			
	As	10	5			
	Au	8	5			
	Ba	1	0.5			
	Be	1	0.5			
	Bi	10	5			
	Cd, Co, Cr, Y,	2	2.5			
	Cu, Sr, Zn	2	1.5			
	Ga, Mn, Nb, Pb	4	5			
	Li, Mo, Sc	2	5			
	Ni	3	5			
	Sn	5	5			
	Ta	40	5			
	Th	6	5			
	U	100	10			
	V	2	3			
	La	2	5			
	Ce	5	5			
Nd	9	5				
Eu	2	0.5				
Ho	4	0.5				
Yb	1	0.5				
HG-AAS using multi-acid digestion	As, Sb	0.6	20 ppm	±20	20	
	Hg	0.02	1.8 ppm	±20	20	
	Se	0.2	0.1	4 ppm	±20	15
	Tl			--	±15	15
				±15	20	
F by ion selective electrode	F	--	--			
Total C	C	0.05%	30	±15	15	
Carbonate C	C	0.01%	10	±15	15	
Total S	S	0.05%	35	±15	15	

^a Upper analytical range may be extended by sample dilution.

^b Percent of spike or known concentration recovered at 5 times the lower limit of detection.

^c RSD: Relative standard deviation.

Table 3b. Correlation coefficients for analytes measured by two different analytical techniques.

Analyte Pair*	Correlation Coefficient
Al ₍₁₎ / Al ₍₂₎	0.999
Fe ₍₁₎ / Fe ₍₂₎	0.998
Mg ₍₁₎ / Mg ₍₂₎	0.998
Ca ₍₁₎ / Ca ₍₂₎	0.999
Na ₍₁₎ / Na ₍₂₎	0.998
K ₍₁₎ / K ₍₂₎	0.999
Ti ₍₁₎ / Ti ₍₂₎	0.973
P ₍₁₎ / P ₍₂₎	0.999
As ₍₁₎ / As ₍₃₎	1.000
Ba ₍₁₎ / Ba ₍₂₎	0.780
Cr ₍₁₎ / Cr ₍₂₎	0.967
Sr ₍₁₎ / Sr ₍₂₎	0.998
Y ₍₁₎ / Y ₍₂₎	0.999

*: Correlation from 77 analyses, except for As (39) and Y (67), which were not detected in some samples.

(1): ICP-AES using multi-acid digest;

(2): ICP-AES using lithium metaborate fusion

(3): HG-Cold Vapor, AAS

Table 4. Major-element oxide and F, C, and S concentrations.

Sample ID ^a	Lithology ^b	Bed Thick (cm)	Cumm Thick ^c (cm from base of MPM)	SiO ₂	Al ₂ O ₃	Fe ₂ O ₃	MgO	CaO	Na ₂ O	K ₂ O	TiO ₂	P ₂ O ₅	MnO	F	Total C	CO ₂	Carb C ^d	Org C ^e	S
				%	%	%	%	%	%	%	%	%	%	ppm	ppm	%	%	%	%
E93	Carbonate	152.4	7833	28.2	1.04	0.60	13.9	22.5	0.36	0.22	0.05	0.78	1007	847	9.1	32.6	8.9	0.2	0.26
E92(4.6-9)	Carbonate	137	7681	22.0	0.74	0.60	14.7	24.5	0.39	0.20	0.03	1.10	866	1260	9.89	34.6	9.44	0.45	0.27
E92(0-4.5)	Carbonate	145	7544	16.3	0.77	0.56	16.3	25.9	0.35	0.2	0.03	0.94	803	888	10.7	37.8	10.32	0.38	0.19
E91	Siliceous	21	7399	56.9	0.66	0.60	7.64	14.3	0.23	0.19	0.05	2.31	377	2090	4.94	17.5	4.78	0.16	0.37
E89-90	Carbonate	46	7378	25.2	0.79	0.51	13.4	23.9	0.42	0.22	0.03	1.88	665	2320	8.88	31.8	8.68	0.2	0.22
Us88	Siliceous	46	7332	55.8	0.64	0.57	6.88	14.3	0.28	0.19	0.05	2.57	391	2840	4.66	16.5	4.5	0.16	0.31
To87(7.1-11)	Siliceous	137	7286	71.5	0.93	0.50	3.22	10.8	0.42	0.31	0.07	3.9	284	3780	2.38	8.15	2.22	0.16	0.35
To87(3.1-7)	Siliceous	114	7149	65.7	0.74	0.51	4.34	12.4	0.36	0.25	0.05	2	328	2260	3.6	12.3	3.36	0.24	0.35
To87(2.26-3)	Siliceous	15	7035	75.1	0.89	0.46	2.85	8.94	0.31	0.29	0.05	1.01	241	1280	2.69	9.15	2.5	0.19	0.32
To87(0-2.25)	Siliceous	69	7020	77.2	0.77	0.36	1.51	9.23	0.35	0.28	0.05	3.12	142	3080	1.77	5.44	1.48	0.29	0.39
To86(5.6-7.5)	Siliceous	91	6951	71.2	2.10	1.00	3.5	8.94	0.4	0.77	0.12	1.58	249	1910	2.71	9	2.46	0.25	0.87
To86(0-5.5)	Siliceous	137	6860	75.1	1.79	0.79	3.02	7.30	0.39	0.69	0.10	1.05	173	1590	2.38	7.58	2.07	0.31	0.75
To85	Siliceous	274	6723	55.6	4.40	1.77	6.48	11.5	0.63	1.55	0.25	1.74	302	2400	4.3	13.9	3.79	0.51	1.46
To83-84	Siliceous	258	6449	60.3	2.38	1.09	5.51	11.8	0.44	0.83	0.12	2.1	262	2640	4.16	13	3.55	0.61	0.99
Rt81	Phosphatic	33	6191	50.1	4.06	1.83	4.05	16.9	0.74	1.41	0.20	8.43	137	9730	3.53	9.03	2.46	1.07	1.94
To80	Siliceous	335	6158	71.5	2.23	0.94	4.53	8.44	0.43	0.75	0.12	1.63	168	1850	3.21	9.4	2.57	0.64	0.78
Rt76-77-To78	Detrital	411	5823	59.5	6.41	2.67	4.25	9.04	0.80	2.19	0.30	2.64	163	2620	4.08	7.68	2.1	1.98	2.69
Rt75	Phosphatic	43	5412	29.3	1.79	1.20	3.88	31.2	0.75	0.5	0.10	18.0	170	15100	3.78	11.4	3.11	0.67	1.45
F73 74	Carbonate	198	5369	9.43	0.62	0.71	16.3	29.7	0.51	0.16	0.05	4.81	510	3450	10.5	36.5	9.96	0.54	0.59
F72	Carbonate	61	5171	12.2	0.38	0.23	15.8	30.4	0.39	0.11	0.02	2.18	207	2580	10.9	38.1	10.4	0.5	0.26
F69-71	Carbonate	259	5110	24.4	0.55	0.34	15.2	24.1	0.30	0.16	0.03	1.40	190	1160	9.52	34.2	9.33	0.19	0.3
F66-68	Carbonate	46	4851	34.7	9.45	3.25	11.3	14.4	1.42	3.06	0.45	0.18	217	2570	6.07	22.2	6.06	0.01	2.35
F64(5.5) 65	Carbonate	274	4805	36.2	0.42	0.26	13.9	19.3	0.22	0.08	0.02	0.21	214	248	8.52	30.5	8.32	0.2	0.13
F64(0-5)	Sand + Carb	228	4531	43.2	5.14	1.09	10.8	15.1	1.40	1.48	0.3	0.2	221	820	6.38	23.1	6.3	0.08	0.64
LS62	Sand + Carb	579	4303	43.4	4.42	1.13	9.3	16.2	1.58	0.98	0.32	0.30	205	506	5.96	21.8	5.95	0.01	1.77
F60	Carbonate	558	3724	32.3	4.67	1.52	4.39	22.1	0.92	1.43	0.28	0.37	121	840	2.98	10.6	2.89	0.09	10
F58-59	Carbonate	98	3166	20.0	1.49	0.57	10.3	29.9	0.43	0.52	0.10	1.6	165	1360	9.01	33.1	9.03	--	2.57

Table 4, continued

Sample ID ^a	Lithology ^b	Bed Thick (cm)	Cumm Thick ^c (cm from base of MPM)	SiO ₂	Al ₂ O ₃	Fe ₂ O ₃	MgO	CaO	Na ₂ O	K ₂ O	TiO ₂	P ₂ O ₅	MnO	F	Total C	CO ₂	Carb C ^d	Org C ^e	S
				%	%	%	%	%	%	%	%	%	%	ppm	ppm	%	%	%	%
LS57	Sand + Carb	398	3068	43.4	0.19	0.13	8.8	21	0.26	0.05	0.02	3.57	94	2860	6.57	23.3	6.36	0.21	0.97
LS56	Siliceous	46	2678	78.1	0.19	0.16	1.28	11	0.24	0.02	0.02	1.95	31	2300	2.65	8.36	2.28	0.37	0.49
LS55	Carbonate	61	2632	26.5	1.06	0.39	15.3	22.8	0.65	0.06	0.08	0.57	208	346	9.42	34.3	9.36	0.06	0.34
M52-54	Phosphatic	161	2571	44.3	1.42	0.74	2.42	25.3	0.88	0.43	0.10	16.1	57	16480	2.26	7.13	1.95	0.31	1.31
M51	Phosphatic	30	2410	27.8	0.79	0.63	0.46	35.1	1.04	0.41	0.07	25.9	15	25890	1.51	3.16	0.86	0.65	1.9
R50	Siliceous	366	2380	70.8	2.46	0.92	4.20	9.14	0.66	0.65	0.15	2.02	84	2270	2.76	9.66	2.64	0.12	0.82
M48-49	Siliceous	101	2014	65.5	4.84	1.86	5.37	8.20	0.90	1.3	0.30	0.69	93	1740	3.1	11.1	3.03	0.07	1.37
M47	Phosphatic	15	1913	43.2	1.13	0.47	0.15	29.5	0.98	0.22	0.07	22.9	14	18340	0.43	0.97	0.26	0.17	1.04
R46	Sand + Carb	98	1898	45.4	1.23	1.07	10.8	17.9	0.39	0.29	0.05	1.31	272	1420	6.74	24	6.55	0.19	0.88
M45	Carbonate	76	1800	14.7	1.57	1.20	16.4	25.5	0.53	0.30	0.08	0.27	319	406	10.9	38.4	10.48	0.42	0.95
M43-44	Phosphatic	92	1724	34.7	3.87	1.39	5.36	24.3	0.85	1.19	0.18	12.8	102	12390	3.76	13.4	3.66	0.1	1.5
M40(.2-.4) 42	Detrital	244	1632	66.1	8.24	1.93	2.55	7.04	2.95	1.72	0.55	1.10	118	1300	2.49	7.06	1.93	0.56	1.5
M36(2.9)-40	Phosphatic	155	1388	37.0	8.18	3.30	4.23	17.3	1.09	2.63	0.38	9.05	170	10510	5.61	8.94	2.44	3.17	3.8
M36(0-1.5)	Carbonate	43	1233	7.53	1.64	0.53	17.7	25.5	0.53	0.40	0.07	0.64	152	410	15.5	39	10.64	4.86	1.5
M35	Detrital	15	1190	45.8	5.97	1.76	8.57	13.1	1.77	1.51	0.38	0.5	271	408	6.52	18.5	5.05	1.47	1.76
M34	Phosphatic	9	1175	55.0	10.8	3.73	1.56	9.15	1.56	3.28	0.57	6.10	167	6790	2.95	1.9	0.52	2.43	3.68
M33	Detrital	30	1166	52.8	7.39	2.27	5.92	10.0	1.67	2.06	0.43	1.01	250	1210	5.37	12.4	3.38	1.99	2.26
M32	Detrital	12	1136	44.3	9.24	3.15	5.12	11.6	0.96	2.82	0.40	3.73	194	3570	5.76	10.2	2.78	2.98	3.13
M30-31	Detrital	85	1124	38.9	6.86	2.27	8.44	14.4	0.92	2.00	0.30	1.70	234	1680	7.61	19	5.19	2.42	2.23
M28-29	Phosphatic	53	1039	23.7	4.38	1.53	9.49	24.2	1.25	1.13	0.22	7.88	158	7250	7.77	21.9	5.98	1.79	1.98
M26-27	Detrital	200	986	37.4	6.42	2.20	8.92	14.0	1.25	1.73	0.3	1.8	191	1740	7.55	19.5	5.32	2.23	2.3
M23-25	Carbonate	128	786	25.2	5.14	1.62	10.8	20.1	0.89	1.48	0.22	3.00	148	2320	11.2	24.5	6.69	4.51	2.43
M21-22	Phosphatic	192	658	21.1	4.33	1.52	9.5	20.8	0.92	1.30	0.22	5.20	132	3290	13.7	21.9	5.98	7.72	3.23
M19-20	Carbonate	229	466	23.5	3.55	1.10	12.3	22.0	1.09	0.93	0.23	2.73	203	1390	10.2	29.8	8.13	2.07	1.53
M16-18	Detrital	98	237	22.7	5.23	1.77	6.83	17.3	0.90	1.72	0.27	4.67	155	3660	19.1	16.8	4.59	14.5	5.2
M14-15	Phosphatic	94	139	15.2	3.67	1.46	9.20	22.8	0.74	1.18	0.18	5.75	141	5720	17.6	22.5	6.14	11.5	4.02
M13	Sand + Carb	15	45	41.7	2.89	0.89	7.43	18.7	0.98	0.67	0.18	0.14	209	106	7.08	23.3	6.36	0.72	1.02
M12(3)	Phosphatic	10	30	2.50	0.49	0.30	1.13	47.4	1.12	0.13	0.03	33.2	26	29160	3.05	6.37	1.74	1.31	1.58

Table 4, continued

Sample ID ^a	Lithology ^b	Bed Thick (cm)	Cumm Thick ^c (cm from base of MPM)	SiO ₂	Al ₂ O ₃	Fe ₂ O ₃	MgO	CaO	Na ₂ O	K ₂ O	TiO ₂	P ₂ O ₅	MnO	F	Total C	CO ₂	Carb C ^d	Org C ^e	S
				%	%	%	%	%	%	%	%	%	%	ppm	ppm	%	%	%	%
M12(2)	Phosphatic	10	20	5.18	0.34	0.16	0.32	48.1	0.9	0.08	0.02	32.3	15	30440	2.63	6.71	1.83	0.8	1.15
M12(1)	Phosphatic	10	10	9.37	0.34	0.13	1.54	45.5	0.74	0.08	0.02	23.4	59	21060	4.88	14.8	4.04	0.84	10
Ws11	Carbonate	122	0	22.0	2.46	0.77	15.67	22.4	0.32	1.01	0.13	0.53	315	681	9.79	35	9.55	0.24	0.69
Ws6-10	Detrital	305	-122	50.7	5.10	1.67	8.84	12.0	0.50	2.10	0.27	0.14	226	715	5.29	19	5.19	0.1	1.28
Ws5	Detrital	101	-427	60.3	8.12	2.75	5.12	6.60	0.7	3.30	0.47	0.11	221	1240	2.87	10.1	2.76	0.11	2.01
Ws4	Carbonate	64	-528	16.4	1.93	0.67	17.6	24.1	0.15	0.83	0.10	0.02	372	263	10.5	37.5	10.23	0.27	2.07
Ws3	Siliceous	58	-592	65.0	2.51	0.67	3	9.64	0.07	1.35	0.12	0.02	119	326	2.52	9.1	2.48	0.04	2.73
Ws2	Carbonate	67	-650	19.0	1.93	0.59	16.0	24.2	0.12	0.88	0.10	0.05	381	419	10.2	36	9.83	0.37	1.9
Ws1	Siliceous	128	-717	69.3	2.72	0.73	2.24	9.32	0.36	1.31	0.2	0.05	80	254	1.78	6.05	1.65	0.13	3.8
M53bmd	Phosphatic	na	na	17.9	5.63	3.37	1.39	29.9	1.17	2.11	0.55	20.6	71	22890	3.57	3.41	0.93	2.64	5.34
M53bst	Phosphatic	na	na	38.9	3.14	0.87	1.69	26.3	1.4	1.1	0.23	17.3	34	18320	1.54	4.66	1.27	0.27	1.46
M53cvug	Siliceous	na	na	62.9	0.25	0.10	1.85	17.6	0.23	0.05	<0.02	0.37	13	3960	4.31	15.6	4.26	0.05	0.1
To84b-pel	Phosphatic	na	na	40.9	4.84	2.20	3.93	21.3	0.97	1.72	0.23	11.2	234	12260	3.38	9.09	2.48	0.9	2.21
To87a-mtx	Siliceous	na	na	67.6	2.25	1.20	2.7	10.6	0.39	0.93	0.13	3.60	252	3690	2.46	7.76	2.12	0.34	1.07
To87c-mtx	Detrital	na	na	60.8	18.5	3.19	0.49	2.1	4.38	2.73	0.30	0.11	2092	424	1.28	0.03	0.01	1.27	0.1
To87e-mtx	Phosphatic	na	na	49.0	1.66	1.40	2.09	23.1	0.61	0.57	0.2	14.8	185	13880	2.02	5.17	1.41	0.61	1.54
To87g-mtx	Carbonate	na	na	86.9	0.43	0.19	1.42	4.79	0.26	0.11	0.02	0.85	154	1210	1.32	4.24	1.16	0.16	0.13
To87i-mtx	Chert	na	na	29.7	0.68	0.70	12.39	23.5	0.3	0.2	0.05	2.66	895	3050	8.32	29.6	8.08	0.24	0.2
To87h-ch	Siliceous	na	na	83.4	1.11	0.47	1.07	6.49	0.39	0.29	0.07	3.80	120	3660	0.83	2.52	0.69	0.14	0.39
To87f-cnod	Siliceous	na	na	72.3	0.62	0.24	1.72	13	0.35	0.17	0.03	1.3	65	2230	2.7	9.19	2.51	0.19	0.19
To87j-cnod	Chert	na	na	92.4	0.42	0.21	0.5	2.9	0.26	0.1	0.02	1.28	209	1430	0.49	1.42	0.39	0.1	0.16
E92b-cnod	Siliceous	na	na	77.4	0.42	0.26	3.25	8.48	0.31	0.13	0.02	0.87	191	1100	2.76	9	2.46	0.3	0.22

^aLetter designations as follows: E = Ervay Member, Park City Formation (PCF); To = Tosi Chert Member, Phosphoria Formation (PF); Retort = Retort Phosphatic Shale Member, PF; F = Franson Member, PCF; US and LS = Upper and Lower Shedhorn Sandstone; M = Meade Peak Member, PF; R = Rex Chert Member, PF; W = Wells; bmd = black massive dolomite (subsample); bst = black siltstone (subsample); cvug = calcite vug (subsample); pel = pellet (subsample); mtx = matrix (subsample); ch = chert (subsample); cnod = conodont (subsample). Formations as described by Sheldon (1963), except Wells Formation interpreted as Grandeur Member, PCF per McKelvey and others (1959). ^bLithologies based on major element chemistries via ordered criteria: chert: > 85% SiO₂; phosphatic: > 5% P₂O₅; sand + carbonate: > 40% SiO₂ & > 25% (MgO + CaO); carbonate: > 25% (MgO + CaO); detrital (non-phosphatic shale, siltstone, or sandstone): > 5% Al₂O₃; siliceous: > 50% SiO₂. ^cCummulative thickness from base of Meade Peak Member.

^dCarbonate carbon. ^eOrganic carbon, calculated as the difference between total and carbonate carbon.

Table 5. Minor-element concentrations in mg kg⁻¹; “<” indicates less than the detection limit given.

Sample ID ^a	Ag	As	Ba	Be	Cd	Co	Cr	Cu	Ga	Hg	Li	Mo	Nb	Ni	Pb	Sb	Sc	Se	Sr	Tl	V	Zn
E93	<2	1	54	<1	<2	<2	13	26	<4	0.94	11	<2	8	7	9	<0.6	<2	1	86	<0.1	18	18
E92(4.6-9)	<2	1.7	31	<1	<2	<2	78	5	<4	1.38	9	<2	8	5	8	<0.6	<2	1.2	107	<0.1	15	15
E92(0-4.5)	<2	0.8	45	<1	<2	<2	44	30	<4	0.75	9	<2	10	4	11	<0.6	<2	1.3	95	<0.1	17	17
E91	<2	2.1	35	<1	<2	<2	15	7	<4	0.07	16	<2	<4	6	18	<0.6	2	3.2	82	<0.1	18	18
E89-90	<2	1.2	38	<1	<2	<2	18	28	<4	1	12	<2	7	3	39	<0.6	<2	2.5	117	<0.1	19	19
Us88	<2	1.9	50	<1	<2	<2	28	38	<4	1.09	17	<2	<4	6	39	<0.6	<2	2.6	106	0.1	19	19
To87(7.1-11)	<2	3.3	57	<1	<2	<2	31	15	<4	0.91	24	<2	<4	6	20	<0.6	2	2	131	0.2	24	24
To87(3.1-7)	<2	2.6	68	<1	<2	<2	27	24	<4	1	18	2	<4	6	8	<0.6	<2	1.4	128	0.2	14	14
To87(2.26-3)	<2	3.4	67	<1	5	<2	56	26	5	0.41	18	2	<4	6	8	<0.6	<2	1.8	87	0.1	13	13
To87(0-2.25)	<2	3.7	60	<1	<2	<2	49	7	<4	0.39	19	8	<4	8	12	<0.6	<2	1.5	125	0.4	13	13
To86(5.6-7.5)	<2	8.4	109	<1	<2	<2	44	26	5	0.5	25	15	<4	11	29	<0.6	2	2.1	104	1.4	26	26
To86(0-5.5)	<2	5	465	<1	<2	<2	34	21	5	0.16	27	6	<4	9	41	<0.6	2	1.6	162	0.7	23	23
To85	<2	5.2	114	<1	<2	3	214	25	11	0.42	44	4	6	22	36	<0.6	5	2.6	111	0.7	56	56
To83-84	<2	2.9	86	<1	<2	<2	77	19	6	0.26	35	2	<4	15	28	<0.6	3	2.2	135	0.4	42	42
Rt81	<2	5.4	121	1	<2	2	136	25	7	0.42	49	5	<4	30	52	<0.6	6	6.7	441	0.8	81	81
To80	<2	1.8	70	<1	<2	<2	34	8	4	0.21	37	3	<4	18	29	<0.6	2	2.2	104	0.2	33	33
Rt76-77-To78	<2	6.2	174	1	<2	4	132	33	11	0.24	59	8	5	71	26	<0.6	7	12.2	169	1.6	105	105
Rt75	<2	8.7	77	<1	4	<2	219	23	8	0.46	26	7	<4	45	20	<0.6	3	7.4	542	2.2	85	85
F73-74	<2	4.2	57	<1	3	<2	98	7	<4	1.1	5	12	6	12	19	0.8	<2	4.5	144	0.7	41	41
F72	<2	1.4	90	<1	<2	<2	32	<2	<4	1.23	5	5	6	6	7	<0.6	<2	2.4	112	0.2	33	33
F69-71	<2	2.4	39	<1	<2	<2	23	9	<4	0.64	9	8	7	8	7	<0.6	<2	1.7	102	0.5	22	22
F66-68	<2	11.6	193	2	<2	9	12	32	12	0.1	55	15	10	27	14	<0.6	10	5.2	85	1.1	81	81
F64(5.5) 65	<2	0.9	37	<1	<2	<2	3	8	<4	0.27	8	3	7	3	6	<0.6	<2	0.8	73	<0.1	6	6
F64(0-5)	<2	1.3	160	<1	<2	4	15	18	8	0.3	28	<2	6	11	13	<0.6	4	1.5	83	0.1	30	30
LS62	<2	1.9	175	<1	<2	4	20	9	9	0.48	13	<2	7	12	15	<0.6	4	2.3	176	0.1	21	21
F60	<2	5.3	249	<1	<2	4	11	15	7	0.28	20	<2	<4	13	9	<0.6	4	0.5	620	0.2	29	29
F58-59	<2	1.9	114	<1	<2	<2	7	2	<4	0.43	7	<2	7	9	9	<0.6	<2	4.4	666	<0.1	13	13
LS57	<2	0.7	27	<1	<2	<2	32	8	<4	1	6	<2	<4	4	6	<0.6	<2	2.8	312	<0.1	6	6
LS56	<2	0.7	50	<1	<2	<2	8	8	<4	0.65	9	<2	<4	<3	6	<0.6	<2	1.8	173	<0.1	4	24
LS55	<2	0.9	25	<1	<2	<2	12	6	<4	0.47	11	<2	8	9	8	<0.6	<2	2.6	88	<0.1	12	46
M52-54	<2	5.4	99	1	15	<2	402	35	7	0.72	20	36	<4	55	17	2	3	19.5	829	1	81	563
M51	<2	8.3	116	<1	48	<2	475	43	8	1.09	14	95	<4	103	19	2.4	3	32.1	1690	1.3	106	1710
R50	<2	9.5	101	<1	3	<2	33	22	6	0.54	24	23	<4	39	18	<0.6	3	3.2	115	1.7	37	102
M48-49	<2	6.6	145	<1	<2	3	62	35	9	0.14	39	11	<4	57	14	0.7	6	6.7	87	2.1	60	66
M47	<2	3.2	158	<1	<2	<2	141	27	<4	0.18	18	22	<4	32	7	1.4	3	4.6	633	0.3	41	127
R46	<2	1.8	56	<1	21	<2	37	13	4	0.35	19	7	6	25	10	<0.6	<2	3.7	114	0.4	30	918
M45	<2	3	601	<1	<2	<2	96	39	<4	0.09	7	4	9	43	7	2.4	<2	8.2	153	0.4	37	30
M43-44	<2	4.6	408	1	3	2	538	41	12	0.36	31	20	5	85	12	3.7	6	17	421	1.3	149	136
M40(.2-.4) 42	2	5	211	<1	<2	3	73	19	11	0.56	12	7	<4	43	17	1	7	34	127	0.9	77	38

Table 5, continued

Sample ID	Ag	As	Ba	Be	Cd	Co	Cr	Cu	Ga	Hg	Li	Mo	Nb	Ni	Pb	Sb	Sc	Se	Sr	Tl	V	Zn
M36(2.9)-40	14	16.7	252	2	147	6	1130	44	17	0.76	35	35	8	127	28	2.1	12	55.1	453	10.7	140	2960
M36(0-1.5)	3	9.9	43	<1	32	<2	241	65	<4	2.22	5	20	9	44	8	4.4	<2	30.1	124	1.2	276	508
M35	2	8.4	177	<1	2	3	147	17	9	1.13	12	4	<4	21	13	0.9	5	9.9	93	1.9	46	52
M34	7	17.1	321	2	9	6	846	41	16	0.65	34	11	8	74	15	1.8	13	27.5	362	4.7	142	329
M33	3	13.9	216	<1	2	5	275	19	11	0.56	18	5	<4	32	11	0.9	7	12.7	117	2.2	66	120
M32	9	20	234	1	25	5	1170	48	19	0.3	37	24	10	106	12	2	12	37.4	230	2.8	161	602
M30-31	6	15.5	169	1	22	5	869	32	14	0.25	28	17	9	76	12	1.6	9	24.9	144	1.9	117	493
M28-29	3	13.2	139	<1	43	3	267	54	8	0.74	14	13	6	55	11	1.6	7	18.2	402	3	93	1120
M26-27	4	23	173	<1	25	4	462	30	12	0.63	18	17	5	50	14	3.9	7	22.2	152	1.4	110	511
M23-25	6	20.6	143	<1	73	3	663	40	13	1.36	15	44	7	115	12	8.8	6	46	211	1.8	336	1100
M21-22	8	31.7	137	<1	235	3	830	80	11	1.29	17	224	8	265	16	28.9	6	143	346	6	1310	2940
M19-20	3	14.8	104	<1	49	3	177	43	8	0.79	7	38	11	82	16	8.6	4	60.3	252	3.5	504	756
M16-18	13	41.8	209	<1	423	<2	1690	198	16	1.14	35	448	10	621	22	26.8	6	287	343	9.7	2690	4580
M14-15	11	26.3	127	<1	149	<2	1490	141	12	1.24	39	190	7	452	16	12.3	6	209	330	5.4	1300	1910
M13	<2	3.7	1020	<1	<2	3	52	6	7	0.99	6	<2	5	10	9	<0.6	2	5.5	289	1.9	20	48
M12(3)	2	6.5	197	<1	26	<2	234	51	<4	0.97	14	32	<4	62	13	4	<2	28.3	1590	1.7	209	534
M12(2)	<2	5.5	234	<1	25	<2	170	47	<4	0.61	12	15	<4	110	12	15.7	<2	22.7	2030	3.2	112	593
M12(1)	<2	3.6	258	<1	21	<2	144	56	4	0.39	9	10	<4	27	8	1.1	<2	13.8	1120	0.7	150	470
Ws11	<2	7.3	149	<1	<2	2	14	6	4	0.19	13	7	9	12	9	0.9	2	12.2	131	1.7	23	68
Ws6-10	<2	8.9	194	<1	<2	4	13	12	8	0.08	19	3	4	18	10	1.2	4	7.9	70	1.5	32	39
Ws5	<2	10.1	277	1	<2	8	28	19	15	0.04	29	3	6	20	17	1.5	7	3.9	59	1.7	51	47
Ws4	<2	2.3	80	<1	<2	<2	8	7	4	0.17	10	3	10	7	10	<0.6	<2	2.9	97	1.2	14	20
Ws3	<2	4.4	1390	<1	<2	2	9	8	5	0.16	8	3	<4	5	13	<0.6	<2	0.8	766	1.1	14	25
Ws2	<2	2.9	172	<1	<2	2	13	6	<4	0.21	10	2	9	6	8	<0.6	<2	2.3	135	0.8	12	27
Ws1	<2	2.2	183	<1	<2	2	9	14	<4	0.26	7	<2	<4	7	8	<0.6	<2	5.3	510	0.4	13	17
M53bmd	5	34.8	208	2	5	6	3240	261	38	1.91	55	32	8	375	90	1.5	4	173	1080	8.2	454	473
M53bst	<2	4	116	2	<2	<2	454	50	7	0.5	26	7	<4	34	19	<0.6	3	27.3	957	0.8	116	166
M53cvug	<2	0.8	24	<1	<2	<2	6	21	<4	0.26	10	<2	<4	<3	84	3.5	<2	1	230	<0.1	9	25
To84b-pel	<2	9.7	147	1	<2	3	239	66	7	0.38	42	11	<4	41	64	<0.6	5	6.9	550	10.7	98	88
To87a-mtx	<2	12.9	99	<1	14	<2	61	72	4	0.39	22	60	<4	25	34	0.7	3	3.8	145	1.2	33	1850
To87c-mtx	3	857	1020	3	28	21	13	149	21	0.11	32	4	9	7	668	3.6	5	0.2	730	1.9	37	2270
To87e-mtx	<2	7.6	75	1	<2	<2	301	62	4	0.55	20	8	<4	18	26	0.8	3	6.1	448	4.7	43	139
To87g-mtx	<2	1.2	38	<1	<2	<2	5	42	<4	1.87	17	<2	<4	<3	5	<0.6	<2	0.3	68	2.2	7	43
To87i-mtx	<2	1.6	38	<1	<2	<2	41	40	<4	1.09	10	<2	6	4	10	<0.6	2	1	113	2.8	19	87
To87h-ch	<2	4.4	57	<1	5	<2	77	65	<4	2.16	28	<2	<4	9	10	0.6	<2	2.7	90	1.9	22	457
To87f-cnod	<2	1	43	<1	<2	<2	24	39	<4	0.71	19	<2	<4	<3	15	<0.6	<2	0.5	156	3	10	38
To87j-cnod	<2	1.3	29	1	<2	<2	10	109	<4	0.26	19	<2	<4	6	10	<0.6	<2	1	70	1.4	10	70
E92b-cnod	<2	0.8	60	<1	<2	<2	16	36	<4	1.04	22	<2	<4	<3	8	<0.6	<2	1.3	132	1.8	7	30

Table 6. Selected rare earth element and Y concentrations in mg kg⁻¹.

Sample	Y	La	Ce	Nd	Eu	Ho	Yb	Ce* ^a
E93	17	13	6	12	<2	<4	1	-0.64
E92(4.6-9)	27	18	10	17	<2	<4	1	-0.56
E92(0-4.5)	22	15	7	16	<2	<4	1	-0.66
E91	53	32	18	30	<2	<4	2	-0.56
E89-90	33	25	9	18	<2	<4	1	-0.72
Us88	63	39	18	33	<2	<4	2	-0.63
To87(7.1-11)	88	54	26	45	<2	<4	3	-0.61
To87(3.1-7)	42	31	13	22	<2	<4	2	-0.65
To87(2.26-3)	20	14	8	9	<2	<4	1	--
To87(0-2.25)	39	29	13	17	<2	<4	1	-0.60
To86(5.6-7.5)	21	15	10	11	<2	<4	1	-0.45
To86(0-5.5)	17	12	7	10	<2	<4	1	-0.53
To85	30	23	24	18	<2	<4	2	-0.26
To83-84	25	18	13	14	<2	<4	1	-0.42
Rt81	69	49	22	30	<2	<4	3	-0.60
To80	27	20	14	14	<2	<4	1	-0.42
Rt76 77 To78	58	45	30	30	<2	<4	3	-0.44
Rt75	181	127	44	90	3	<4	7	-0.73
F73-74	44	28	13	23	<2	<4	2	-0.62
F72	27	16	7	18	<2	<4	1	-0.70
F69-71	25	15	9	19	<2	<4	1	-0.58
F66-68	15	16	30	22	<2	<4	1	-0.10
F64(5.5) 65	4	4	6	9	<2	<4	1	--
F64(0-5)	8	17	30	16	<2	<4	1	-0.06
LS62	17	25	40	22	<2	<4	1	-0.09
F60	16	19	27	21	<2	<4	1	-0.18
F58-59	41	28	19	30	<2	<4	1	-0.50
LS57	98	58	18	43	<2	<4	4	-0.78
LS56	62	35	12	27	<2	<4	2	-0.75
LS55	20	10	5	12	<2	<4	1	-0.65
M52-54	423	270	70	167	6	7	15	-0.84
M51	728	461	113	287	11	12	26	-0.87
R50	46	35	21	30	<2	<4	2	-0.52
M48-49	22	15	22	18	<2	<4	1	-0.18
M47	204	164	70	101	4	<4	7	-0.62
R46	23	20	7	14	<2	<4	1	-0.73
M45	10	9	8	11	<2	<4	1	-0.40
M43-44	187	149	39	76	3	<4	7	-0.82
M40(.2-.4) 42	25	28	35	24	<2	<4	2	-0.20
M36(2.9)-40	127	102	45	55	2	<4	5	-0.60
M36(0-1.5)	9	9	7	10	<2	<4	1	-0.44
M35	12	13	25	18	<2	<4	1	-0.09
M34	46	50	46	37	<2	<4	3	-0.31

Sample	Y	La	Ce	Nd	Eu	Ho	Yb	Ce*
M33	20	20	32	20	<2	<4	1	-0.11
M32	42	38	33	28	<2	<4	2	-0.34
M30-31	34	27	23	25	<2	<4	2	-0.38
M28-29	68	59	25	34	<2	<4	3	-0.62
M26-27	24	24	26	23	<2	<4	1	-0.28
M23-25	26	27	20	19	<2	<4	1	-0.40
M21-22	76	58	24	33	<2	<4	4	-0.63
M19-20	26	26	24	21	<2	<4	1	-0.32
M16-18	120	98	37	57	2	<4	7	-0.67
M14-15	137	101	27	49	2	<4	7	-0.80
M13	4	5	10	11	<2	<4	1	-0.17
M12(3)	221	135	21	88	2	<4	8	-1.07
M12(2)	479	332	66	261	9	8	18	-0.99
M12(1)	132	87	16	56	<2	<4	5	-1.00
Ws11	11	8	11	14	<2	<4	1	-0.28
Ws6-10	6	7	13	11	<2	<4	1	-0.13
Ws5	6	10	19	13	<2	<4	1	-0.08
Ws4	3	2	7	9	<2	<4	1	-0.12
Ws3	3	2	5	9	<2	<4	1	--
Ws2	3	2	5	9	<2	<4	1	--
Ws1	3	3	6	9	<2	<4	1	--
M53bmd	419	73	37	37	<2	<4	4	-0.53
M53bst	484	36	15	24	<2	<4	2	-0.64
M53cvu	11	48	23	37	<2	<4	2	-0.60
g								
To84b-pel	89	18	10	15	<2	<4	1	-0.55
To87f-cnod	40	29	14	18	<2	<4	2	-0.57
To87h-ch	16	40	65	26	<2	<4	2	-0.05
To87j-cnod	270	209	77	119	5	4	8	-0.68
To87a-mtx	17	11	5	9	<2	<4	1	--
To87c-mtx	72	45	17	36	<2	<4	3	-0.71
To87e-mtx	75	12	7	10	<2	<4	1	-0.53
To87g-mtx	46	285	78	186	8	7	16	-0.82
To87i-mtx	30	318	83	190	8	8	18	-0.83
E92b-cnod	18	6	<5	<9	<2	<4	1	--

^a Ce* = Cerium anomaly: $\log [3 \times \text{WSA Ce} / (2 \times \text{WSA La} + \text{WSA Nd})]$ where WSA represents the measured element concentration divided by the world shale average concentration.

Table 7. Gold, platinum, and palladium concentrations ($\mu\text{g kg}^{-1}$) in select samples.

Sample ID	Au	Pt	Pd
Us88	3	<5	2
To87(7.1-11)	1	<5	2
To87(3.1-7)	1	<5	2
To87(2.26-3)	<1	<5	2
To87(0-2.25)	1	<5	2
To86(5.6-7.5)	1	<5	2
To86(0-5.5)	1	<5	2
To85	1	<5	3
To83-84	<1	<5	2
Rt81	<1	<5	3
To80	1	<5	2
Rt76-77-To78	2	<5	3
Rt75	3	<5	3
LS55	1	<5	3
M52-54	2	<5	3
M51	3	<5	3
R50	2	<5	3
M48-49	1	<5	5
M47	2	<5	7
R46	2	<5	8
M45	<1	<5	4
M43-44	1	<5	5
M40(.2-.4) 42	2	<5	4
M36(2.9)-40	2	<5	5
M36(0-1.5)	2	<5	7
M35	1	<5	3
M34	1	<5	9
M33	5	<5	3
M32	3	<5	9
M30-31	3	<5	7
M28-29	1	<5	4
M26-27	1	<5	3
M23-25	3	<5	8
M21-22	7	<5	10
M19-20	7	<5	8
M16-18	16	<5	15
M14-15	9	9	16
M13	4	<5	7
M12(3)	3	5	7
M12(2)	3	<5	4
M12(1)	2	<5	4
Ws11	14	<5	4

Table 8. Correlation coefficients for the log concentrations of major and minor elements.

	SiO ₂	Al ₂ O ₃	Fe ₂ O ₃	MgO	CaO	Na ₂ O	K ₂ O	TiO ₂	P ₂ O ₅	MnO	F	Carb C	Org C
SiO ₂	1.00												
Al ₂ O ₃	0.15	1.00											
Fe ₂ O ₃	0.12	0.94	1.00										
MgO	-0.24	0.13	0.19	1.00									
CaO	-0.78	-0.26	-0.18	0.26	1.00								
Na ₂ O	-0.13	0.65	0.60	-0.19	0.02	1.00							
K ₂ O	0.16	0.97	0.92	0.12	-0.24	0.53	1.00						
TiO ₂	0.16	0.97	0.94	0.12	-0.20	0.63	0.95	1.00					
P ₂ O ₅	-0.24	-0.16	-0.03	-0.40	0.39	0.33	-0.15	-0.10	1.00				
MnO	0.10	0.20	0.28	0.63	-0.22	-0.13	0.18	0.13	-0.44	1.00			
F	-0.21	-0.10	0.01	-0.50	0.37	0.29	-0.05	-0.05	0.91	-0.52	1.00		
Carb C	-0.37	-0.18	-0.12	0.84	0.53	-0.33	-0.15	-0.14	-0.19	0.26	-0.28	1.00	
Org C	-0.36	0.30	0.34	0.02	0.18	0.36	0.29	0.25	0.43	-0.02	0.27	-0.04	1.00
S	-0.20	0.65	0.64	0.04	0.23	0.42	0.69	0.70	0.14	-0.32	0.22	0.06	0.40
As	-0.11	0.73	0.71	-0.15	-0.15	0.63	0.71	0.68	0.17	0.04	0.21	-0.42	0.57
Ba	-0.07	0.65	0.55	-0.16	-0.09	0.46	0.65	0.60	-0.15	-0.10	-0.04	-0.29	0.20
Cr	-0.31	0.43	0.50	-0.10	0.32	0.56	0.43	0.45	0.68	-0.25	0.60	-0.07	0.75
Cu	-0.06	0.29	0.31	-0.39	-0.09	0.42	0.28	0.26	0.44	-0.17	0.46	-0.44	0.43
Hg	-0.26	-0.27	-0.22	0.03	0.29	0.07	-0.28	-0.23	0.45	-0.07	0.25	0.14	0.40
Li	0.39	0.55	0.59	-0.28	-0.36	0.37	0.57	0.54	0.28	-0.05	0.40	-0.42	0.12
Mn	0.10	0.20	0.28	0.63	-0.22	-0.13	0.18	0.13	-0.44	1.00	-0.52	0.26	-0.02
Mo	-0.36	0.39	0.42	-0.09	0.27	0.44	0.41	0.39	0.49	-0.34	0.49	-0.07	0.62
Ni	-0.36	0.59	0.62	-0.05	0.28	0.62	0.58	0.61	0.48	-0.32	0.46	-0.05	0.63
Pb	0.17	0.37	0.40	-0.25	-0.26	0.34	0.37	0.33	0.14	0.18	0.25	-0.49	0.18
Se	-0.42	0.42	0.45	0.04	0.39	0.50	0.43	0.47	0.48	-0.37	0.44	0.12	0.68
Sr	-0.37	0.07	0.05	-0.53	0.43	0.36	0.10	0.08	0.51	-0.56	0.61	-0.39	0.32
Tl	-0.28	0.66	0.65	-0.03	0.15	0.51	0.70	0.67	0.23	-0.21	0.29	-0.08	0.59
V	-0.43	0.54	0.55	0.01	0.30	0.61	0.54	0.54	0.48	-0.22	0.46	-0.01	0.70
Y	-0.20	-0.13	-0.01	-0.47	0.37	0.34	-0.12	-0.06	0.94	-0.47	0.91	-0.30	0.32
Zn	-0.22	0.31	0.33	-0.27	0.08	0.45	0.30	0.28	0.54	-0.20	0.48	-0.31	0.67
La	-0.19	0.02	0.12	-0.49	0.32	0.51	0.01	0.08	0.91	-0.44	0.89	-0.37	0.35
Ce	-0.05	0.44	0.50	-0.39	0.14	0.76	0.42	0.50	0.61	-0.31	0.63	-0.43	0.32
Nd	-0.28	0.04	0.14	-0.45	0.41	0.50	0.05	0.12	0.82	-0.46	0.83	-0.32	0.31

Table 8, continued

	S	As	Ba	Cr	Cu	Hg	Li	Mn	Mo	Ni	Pb	Se	Sr	Tl	V
S	1.00														
As	0.53	1.00													
Ba	0.57	0.60	1.00												
Cr	0.61	0.59	0.30	1.00											
Cu	0.23	0.54	0.18	0.55	1.00										
Hg	-0.07	-0.06	-0.34	0.36	0.21	1.00									
Li	0.32	0.44	0.22	0.36	0.49	-0.22	1.00								
Mn	-0.32	0.04	-0.10	-0.25	-0.17	-0.07	-0.05	1.00							
Mo	0.58	0.69	0.34	0.75	0.49	0.15	0.29	-0.34	1.00						
Ni	0.76	0.70	0.46	0.85	0.53	0.09	0.42	-0.32	0.86	1.00					
Pb	0.02	0.52	0.23	0.19	0.41	-0.14	0.50	0.18	0.18	0.18	1.00				
Se	0.70	0.54	0.31	0.84	0.44	0.25	0.20	-0.37	0.79	0.90	0.04	1.00			
Sr	0.45	0.38	0.44	0.49	0.38	0.14	0.07	-0.56	0.44	0.46	0.27	0.43	1.00		
Tl	0.77	0.79	0.64	0.69	0.37	-0.04	0.34	-0.21	0.81	0.84	0.25	0.77	0.44	1.00	
V	0.67	0.71	0.40	0.84	0.59	0.21	0.36	-0.22	0.85	0.93	0.25	0.88	0.45	0.79	1.00
Y	0.16	0.20	-0.10	0.63	0.48	0.39	0.33	-0.47	0.46	0.47	0.21	0.45	0.60	0.22	0.45
Zn	0.38	0.72	0.26	0.72	0.63	0.29	0.30	-0.20	0.76	0.70	0.28	0.61	0.48	0.61	0.71
La	0.23	0.32	0.02	0.67	0.54	0.35	0.38	-0.44	0.50	0.54	0.27	0.49	0.63	0.29	0.53
Ce	0.46	0.55	0.30	0.65	0.47	0.09	0.50	-0.31	0.49	0.64	0.35	0.52	0.53	0.47	0.58
Nd	0.31	0.32	0.10	0.64	0.45	0.30	0.31	-0.46	0.48	0.56	0.21	0.52	0.66	0.35	0.52

	Y	Zn	La	Ce	Nd
Y	1.00				
Zn	0.51	1.00			
La	0.97	0.56	1.00		
Ce	0.71	0.48	0.83	1.00	
Nd	0.93	0.48	0.96	0.85	1.00

Note: All values rounded to nearest hundredth. Only those elements detected in at least 67% of the samples are included; samples with non-detects set to 0.5 the detection value for calculation of correlation coefficients.
 Carb C = carbonate carbon; Org C = organic carbon.

Table 9. World shale average, modern marine plankton, and seawater concentrations of selected elements.

	World Shale Average¹	Deep Seawater²	Marine Plankton³
Major Oxides (wt %)			
Al₂O₃	15.1	--	--
Fe₂O₃	6.84	--	--
MgO	2.49	--	--
CaO	3.09	--	--
Na₂O	1.3	--	--
K₂O	3.19	--	--
P₂O₅	0.16	--	--
SiO₂	58.4	--	--
TiO₂	0.77	--	--
	(ppm)	(ppb)	(ppm)
Cd	0.3	0.10	12
Cr	90	0.22	2.0
Cu	45	0.18	11
Mo	2.6	10.6	2
Ni	68	0.59	7.5
Se	0.6	0.13	3.0
U	3.7	3.00	<1
V	130	1.80	3.0
Zn	95	0.52	110

¹ World Shale Averages from Turekian and Wedepohl (1961)

² Deep seawater values from Boyle et al. (1976; 1977), and Bruland and Franks (1983).

³ Marine plankton values from Martin and Knauer (1973), Brumsack (1986), and Collier (1984).

Table 10. Formulas used to calculate the normative components from measured major-element oxide contents (wt %).

Sedimentary Component	Normative Formula
Terrigenous Detritus	$6.62 \times \text{Al}_2\text{O}_3$
Organic Matter	Organic Carbon $\times 1.53$
Apatite	$(\text{P}_2\text{O}_5 - 0.008 \times \text{Al}_2\text{O}_3) \times 2.38$
Biogenic Silica	$\text{SiO}_2 - 4.0 \times \text{Al}_2\text{O}_3$
Dolomite	$(\text{MgO} - 0.072 \times \text{Al}_2\text{O}_3) \times 4.57$
Calcite	$(\text{CaO} - 0.15 \times \text{Al}_2\text{O}_3 - 0.30 \times \text{Dolomite} - 0.556 \times \text{Apatite}) \times 1.78$

- Terrigenous detritus constant determined via graphical relationship of CaO and alumina.
- Correction for terrigenous fraction of SiO₂ determined via graphical relationship with alumina.
- Corrections for P₂O₅, MgO, and CaO taken from oxide:alumina relationships established for Meade Peak by Medrano and Piper (1995).
- Constant for organic matter based on average C content of 65.2% in western Wyoming Phosphoria kerogens (Powell et al., 1972).

Table 11. Major components in composite samples from the Lakeridge core. All values in wt %, calculated from major-element-oxide contents and the formulas in Table 9.

Sample	Detritus	Apatite	Dolomite	Calcite	Bio-Silica	Org. Matter	Total
E93	6.88	1.83	63.0	3.91	24.1	0.31	100.0
E92(4.6-9)	4.88	2.60	67.0	4.57	19.1	0.69	98.8
E92(0-4.5)	5.13	2.22	74.0	3.62	13.2	0.58	98.8
E91	4.38	5.50	34.7	1.00	54.3	0.25	100.1
E89 90	5.26	4.46	61.1	4.89	22.0	0.31	98.1
Us88*	4.25	6.10	31.2	2.30	53.3	0.25	97.4
To87(7.1-11)	6.13	9.25	14.4	2.08	67.8	0.25	99.9
To87(3.1-7)	4.88	5.44	19.6	5.90	62.7	0.37	98.9
To87(2.26-3)	5.88	2.38	12.7	6.42	71.5	0.29	99.3
To87(0-2.25)	5.13	7.40	6.64	5.31	74.1	0.44	99.1
To86(5.6-7.5)	13.9	3.72	15.2	3.43	62.9	0.38	99.5
To86(0-5.5)	11.9	2.47	13.2	2.93	67.9	0.48	98.9
To85	29.2	4.06	28.2	0.10	38.0	0.78	100.3
To83-84	15.8	4.86	24.4	2.38	50.8	0.94	99.1
Rt81	26.9	20.0	17.2	--	33.8	1.64	99.5
To80	14.8	3.83	20.0	--	62.5	0.98	102.1
Rt76-77-o78	42.4	6.15	17.3	--	33.9	3.04	102.8
Rt75	11.9	42.9	17.1	3.34	22.1	1.03	98.4
F73-74	4.13	11.4	74.1	1.19	6.94	0.83	98.7
F72	2.50	5.17	72.0	9.89	10.7	0.77	101.0
F69-71	3.63	3.32	69.2	1.94	22.2	0.29	100.6
F66-68	62.6	0.26	48.7	--	--	0.02	111.5
F64(5.5) 65	2.75	0.48	63.1	--	34.5	0.31	101.2
F64(0-5)	34.0	0.28	47.5	--	22.7	0.12	104.6
LS62*	29.3	0.62	41.0	4.91	25.7	0.02	101.6
F60**	30.9	0.78	18.6	3.90	13.6	0.14	99.2
F58-59	9.89	3.79	46.6	24.0	14.0	0.00	98.2
LS57*	1.25	8.50	40.1	7.19	42.7	0.32	100.0
LS56*	1.25	4.63	5.77	12.2	77.3	0.57	101.7
LS55*	7.01	1.34	69.7	1.3	22.3	0.09	101.7
M52-54	9.38	38.3	10.6	1.05	38.6	0.48	98.4
M51	5.26	61.6	1.86	0.32	24.6	1.00	94.7
R50	16.3	4.75	18.4	0.97	61.0	0.18	101.5
M48-49	32.0	1.54	23.0	--	46.1	0.11	102.8
M47	7.51	54.4	0.31	--	38.7	0.26	101.2
R46	8.13	3.09	48.7	2.14	40.4	0.29	102.8
M45	10.4	0.62	74.6	3.93	8.38	0.64	98.6
M43-44	25.7	30.5	23.2	--	19.2	0.15	98.6
M40(.2-.4) 42	54.6	2.46	8.96	3.04	33.2	0.86	103.0
M36(2.9)-40	54.2	21.4	16.6	--	4.28	4.86	101.4
M36(0-1.5)	10.9	1.50	80.6	--	0.96	7.45	101.3
M35	39.5	0.98	37.2	0.61	21.9	2.25	102.5
M34	71.7	14.3	3.56	--	11.7	3.73	105.0
M33	48.9	2.26	24.6	0.30	23.3	3.05	102.5
M32	61.2	8.71	20.4	--	7.33	4.57	102.2
M30-31	45.4	3.90	36.3	0.30	11.5	3.71	101.2
M28-29	29.0	18.7	41.9	0.76	6.21	2.75	99.3
M26-27	42.5	4.24	38.7	--	11.7	3.42	100.6

Table 11, continued

Sample	Detritus	Apatite	Dolomite	Calcite	Bio-Silica	Org. Matter	Total
M23-25	34.0	7.05	47.8	1.66	4.69	6.92	102.1
M21-22	28.7	12.3	41.8	1.18	3.79	11.8	99.5
M19-20	23.5	6.42	55.0	2.04	9.32	3.17	99.5
M16-18	34.7	11.0	29.5	2.61	1.74	22.3	101.8
M14-15	24.3	13.6	40.9	4.03	0.55	17.6	100.9
M13	19.1	0.27	33.0	14.5	30.2	1.10	98.2
M12(3)	3.25	79.1	4.99	3.35	0.54	2.01	93.2
M12(2)	2.25	76.9	1.33	8.77	3.82	1.23	94.3
M12(1)	2.25	55.6	6.94	22.1	8.01	1.29	96.2
Ws11	16.3	1.21	70.8	--	12.2	0.37	100.9
Ws6-10	33.8	0.23	38.7	--	30.3	0.15	103.2
Ws5	53.8	0.12	20.7	--	27.8	0.17	102.7
Ws4	12.8	0.02	79.7	--	8.68	0.41	101.6
Ws3*	16.6	0.01	14.3	8.73	55.0	0.06	94.8
Ws2	12.8	0.07	72.5	3.27	11.3	0.57	100.4
Ws1*	18.0	0.06	9.34	10.8	58.4	0.20	96.8
M53bmd	37.3	49.0	4.74	0.76	--	4.05	95.8
M53bst	20.8	41.1	7.00	1.56	26.4	0.41	97.2
M53cvug	1.63	0.87	8.71	25.7	61.9	0.08	98.9
To84b-pel	32.0	26.5	16.4	1.51	21.5	1.38	99.3
To87f-cnod	4.13	5.44	7.68	12.7	69.8	0.29	100.1
To87h-ch	7.38	9.03	4.71	--	79.0	0.21	100.3
To87j-cnod	2.75	3.05	2.14	0.95	90.8	0.15	99.8
To87a-mtx	14.9	8.52	12.1	3.33	58.6	0.52	98.0
To87c-mtx***	122.5	--	--	--	--	1.95	124.4
To87e-mtx	11.0	35.3	9.38	0.69	42.3	0.94	99.6
To87g-mtx	2.88	2.01	6.60	2.84	85.1	0.25	99.7
To87i-mtx	4.50	6.31	58.7	3.63	27.0	0.37	100.6
E92b-cnod	2.75	2.06	14.7	4.98	75.8	0.46	100.8

* Samples denoted by “*” may contain sorted silica-rich sand which, due to low Al₂O₃ content, is calculated as “biogenic silica” when actually present as detrital grains.

** Calculated CO₂ for sample F60 is approximately 2 x the measured CO₂; the two will match assuming a calcite content of 3.9%. The disparity in CO₂ values in this sample and high total in F66-68 due to large amounts of anhydrite not accounted for in this model.

*** The component model does not adequately explain TO87c-mtx. The total for this sample is not included in calculating average component total (99.95%).

Table 12. Principal component analysis of log-normalized concentration data from Lakeridge core samples. Orthogonal varimax transformation using StatView™ software. Values of 0.40 and greater are in bold.

	Variance Proportion ^a :	0.407	0.195	0.121	0.059	0.049	0.037
Analytes	Communalities	Factor 1	Factor 2	Factor 3	Factor 4	Factor 5	Factor 6
SiO ₂	0.90	0.051	0.067	-0.926	0.088	-0.215	-0.177
Al ₂ O ₃	0.99	-0.055	0.951	-0.070	0.025	0.030	0.063
Fe ₂ O ₃	0.97	0.136	0.945	-0.083	0.195	0.006	0.140
MgO	0.96	-0.277	0.252	0.320	0.735	-0.015	0.175
CaO	0.95	0.395	0.064	0.846	0.186	-0.187	-0.007
Na ₂ O	0.92	0.430	0.644	0.192	-0.120	-0.047	0.248
K ₂ O	0.98	-0.052	0.942	-0.102	0.038	0.034	-0.006
TiO ₂	0.98	0.079	1.000	-0.091	0.107	-0.065	-0.022
P ₂ O ₅	0.96	0.891	-0.158	-0.084	0.158	0.217	-0.009
MnO	0.93	-0.262	0.089	0.113	0.395	-0.021	0.751
F	0.96	0.926	-0.002	-0.054	0.000	0.007	-0.070
Carbonate C	0.97	-0.138	0.059	0.340	0.742	-0.052	-0.181
Organic C	0.86	-0.171	-0.088	0.057	0.019	0.982	0.119
S	0.92	0.056	0.786	0.134	-0.002	0.093	-0.463
As	0.93	-0.131	0.454	0.052	-0.334	0.546	0.248
Ba	0.85	-0.308	0.688	0.369	-0.611	-0.053	-0.043
Cr	0.94	0.405	0.301	0.007	0.165	0.560	-0.072
Cu	0.72	0.175	-0.059	-0.305	-0.187	0.660	0.132
Hg	0.70	0.177	-0.543	0.000	0.295	0.619	0.154
Li	0.85	0.549	0.524	-0.649	0.168	-0.051	-0.043
Mo	0.90	0.044	0.211	0.016	-0.052	0.716	-0.221
Ni	0.97	0.231	0.540	0.068	0.056	0.470	-0.226
Pb	0.71	0.238	0.226	0.001	-0.307	0.011	0.660
Se	0.92	0.166	0.363	0.107	0.152	0.567	-0.312
Sr	0.95	0.312	0.130	0.523	-0.659	0.012	0.002
V	0.95	0.159	0.401	0.135	0.059	0.615	-0.057
Y	0.99	0.992	-0.066	-0.040	0.059	0.046	0.027
Zn	0.86	-0.006	-0.086	-0.105	-0.210	0.911	0.053
La	0.99	0.995	0.082	0.003	-0.001	0.009	0.096
Ce	0.97	0.893	0.593	0.049	-0.034	-0.231	0.117
Nd	0.98	0.989	0.212	0.178	-0.039	-0.147	0.066

n = 75

^a The variance proportion is an estimate of the proportion of variance inherent in the dataset which is accounted for by each factor.

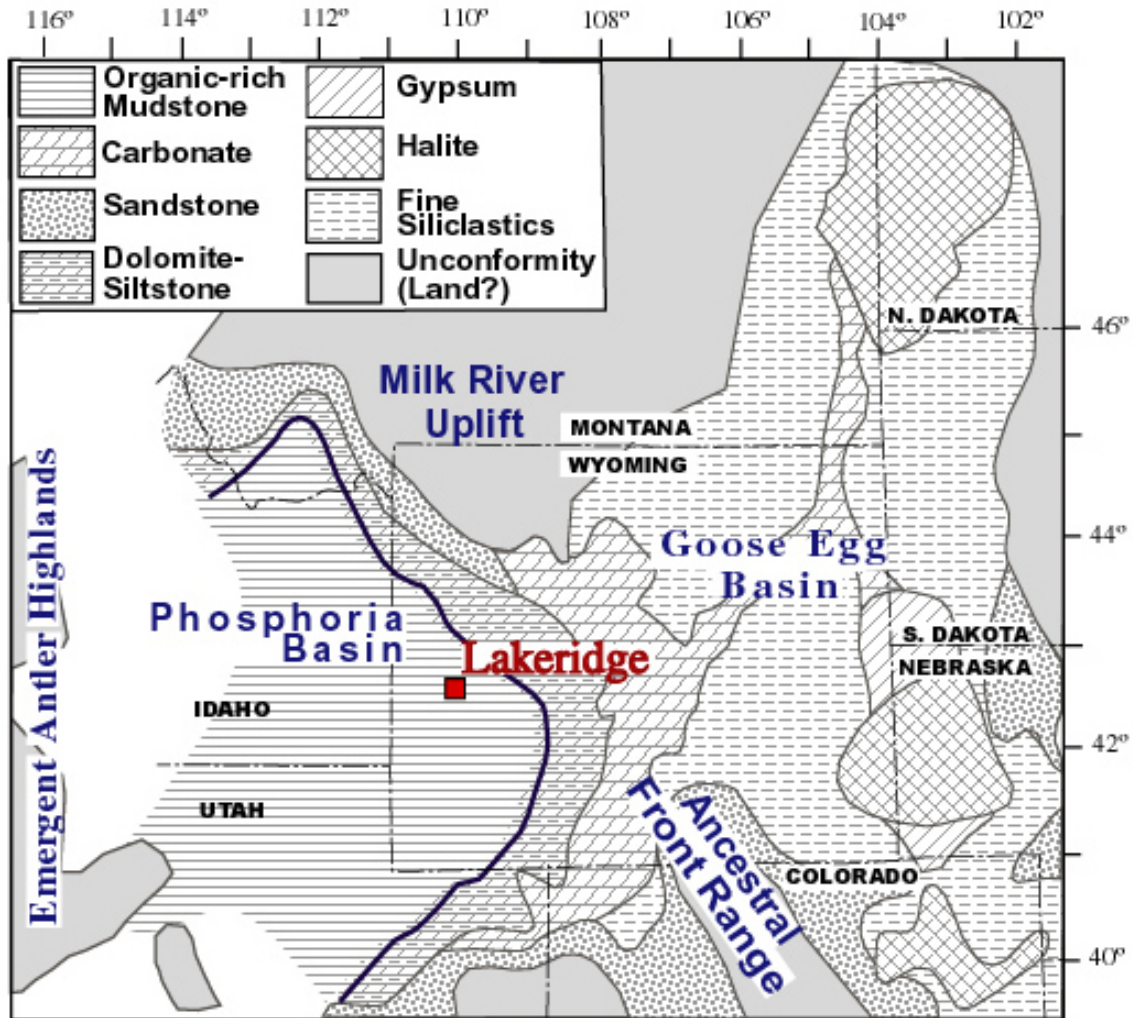


Figure 1. Map showing location of Lakeridge core in context of Permian paleogeography with present latitude and longitude coordinates. The eastern and northern extent of the Phosphoria Basin is shown by bold line. Major tectonic features include the remnant Antler Highlands to the west, the Ancestral Front Range to the southeast, and the Milk River Uplift to the North. The Phosphoria Basin is separated from shallow, evaporite basins in eastern Wyoming, North and South Dakota, and Nebraska by a carbonate platform lying east of the Lakeridge section.

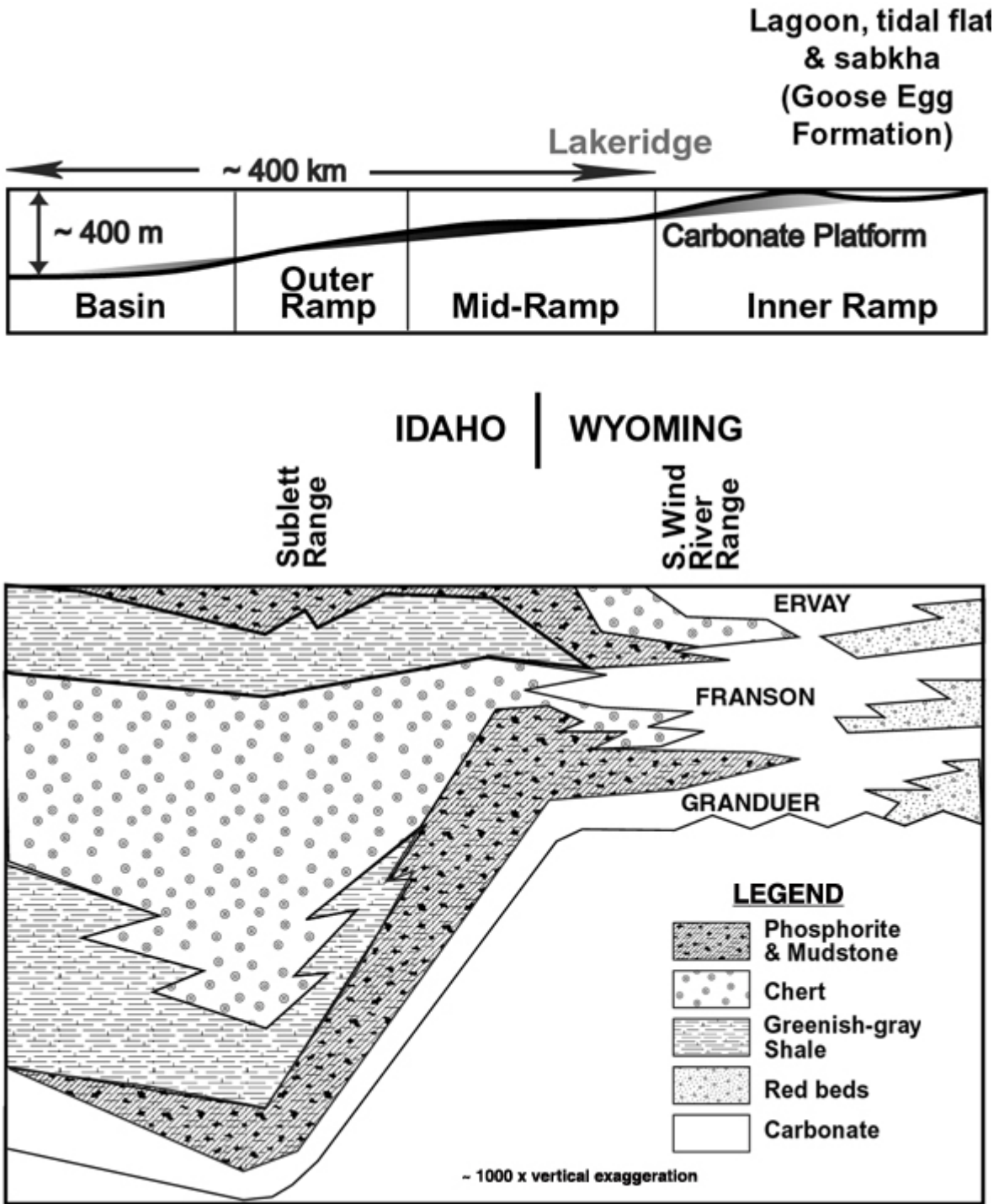


Figure 2. Position of the Lakeridge section on the upper slopes of a low-angle carbonate ramp and generalized lithologic relationships of the Park City Formation (PCF) and Phosphoria Formation (PF) (modified from Burchette and Wright, 1992 and Maughan, 1994).

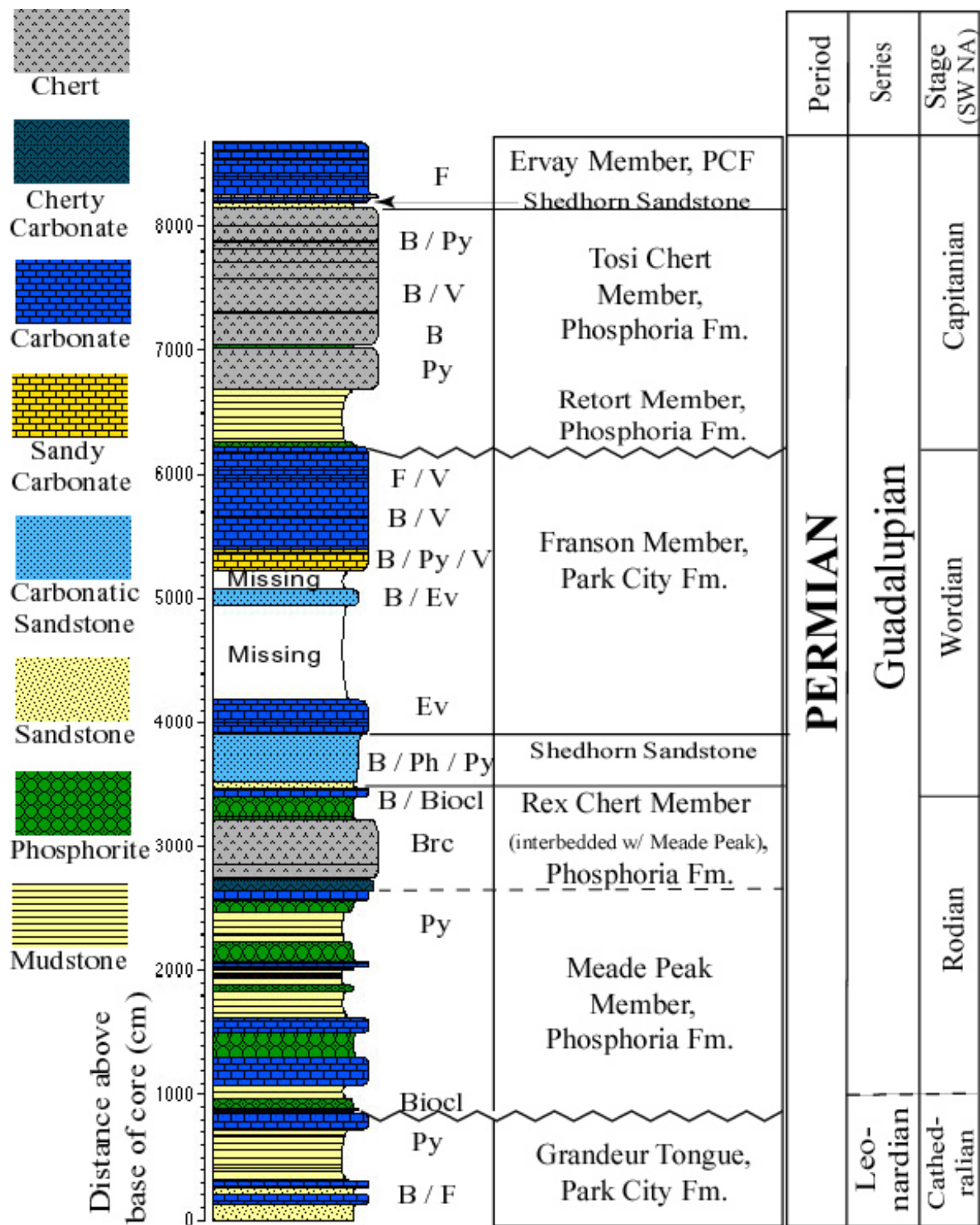


Figure 3. Generalized stratigraphic column of the Park City Formation (PCF), Phosphoria Formation, and Shedhorn Sandstone in the Lakeridge core. Series and stage names from Ross and Ross (1995). B = burrowed; Biocl = bioclastic; Brc = brecciated; Ev = evaporates; F = fossiliferous; Ph = phosphatic; Py = pyritic; V = vuggy.

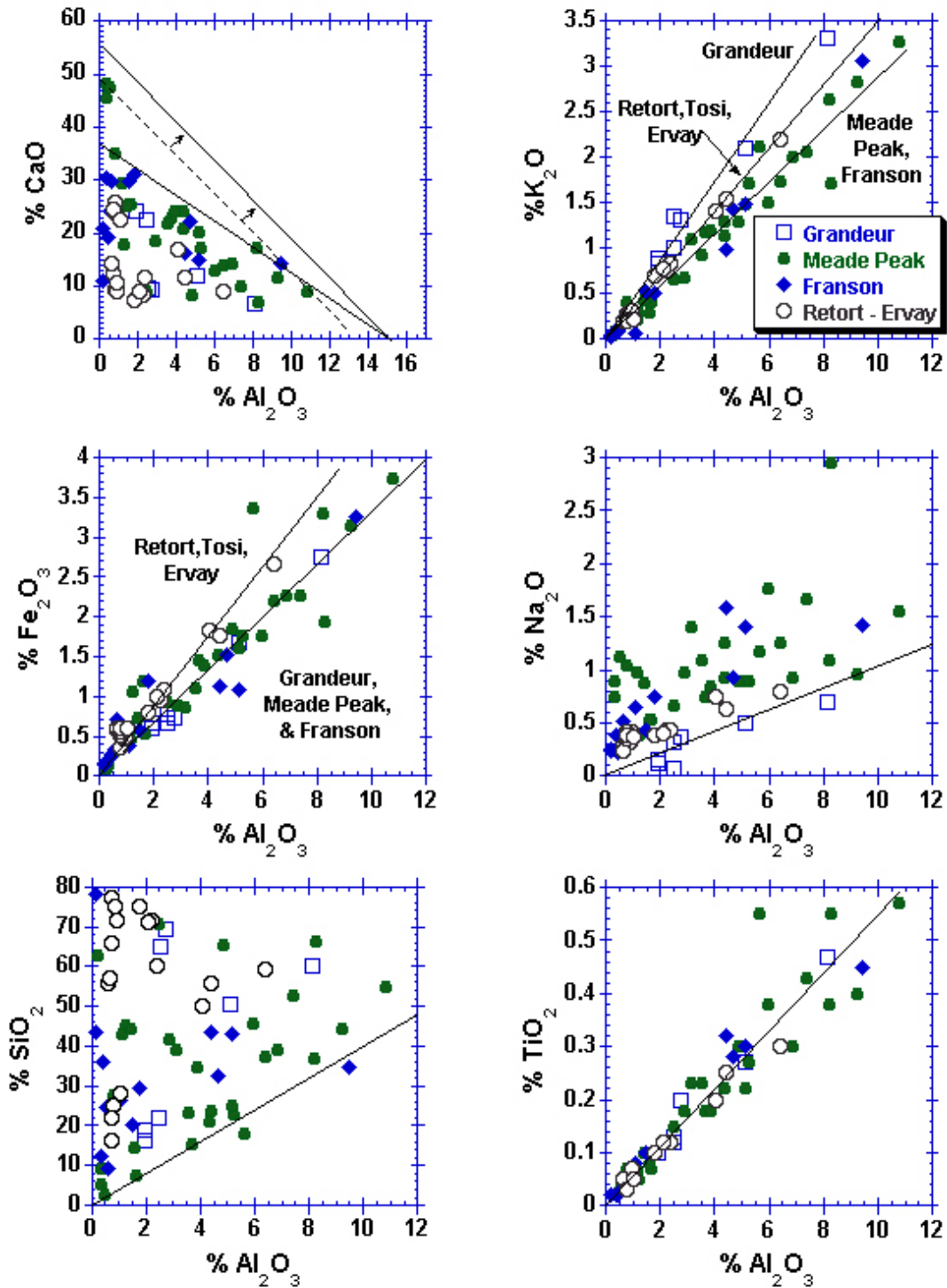


Figure 4. Scatter plots showing major-element oxides that occur almost exclusively in the terrigenous fraction (Al_2O_3 , Fe_2O_3 , K_2O , TiO_2) and others that occur dominantly in other phases but also in the terrigenous fraction (Na_2O , and SiO_2). The detrital Al_2O_3 content (15.1%) is calculated based on extrapolation of the maxima (mixing) line in the CaO vs Al_2O_3 plot to near-zero percent CaO ; see text for discussion of minima, maxima, and regression lines.

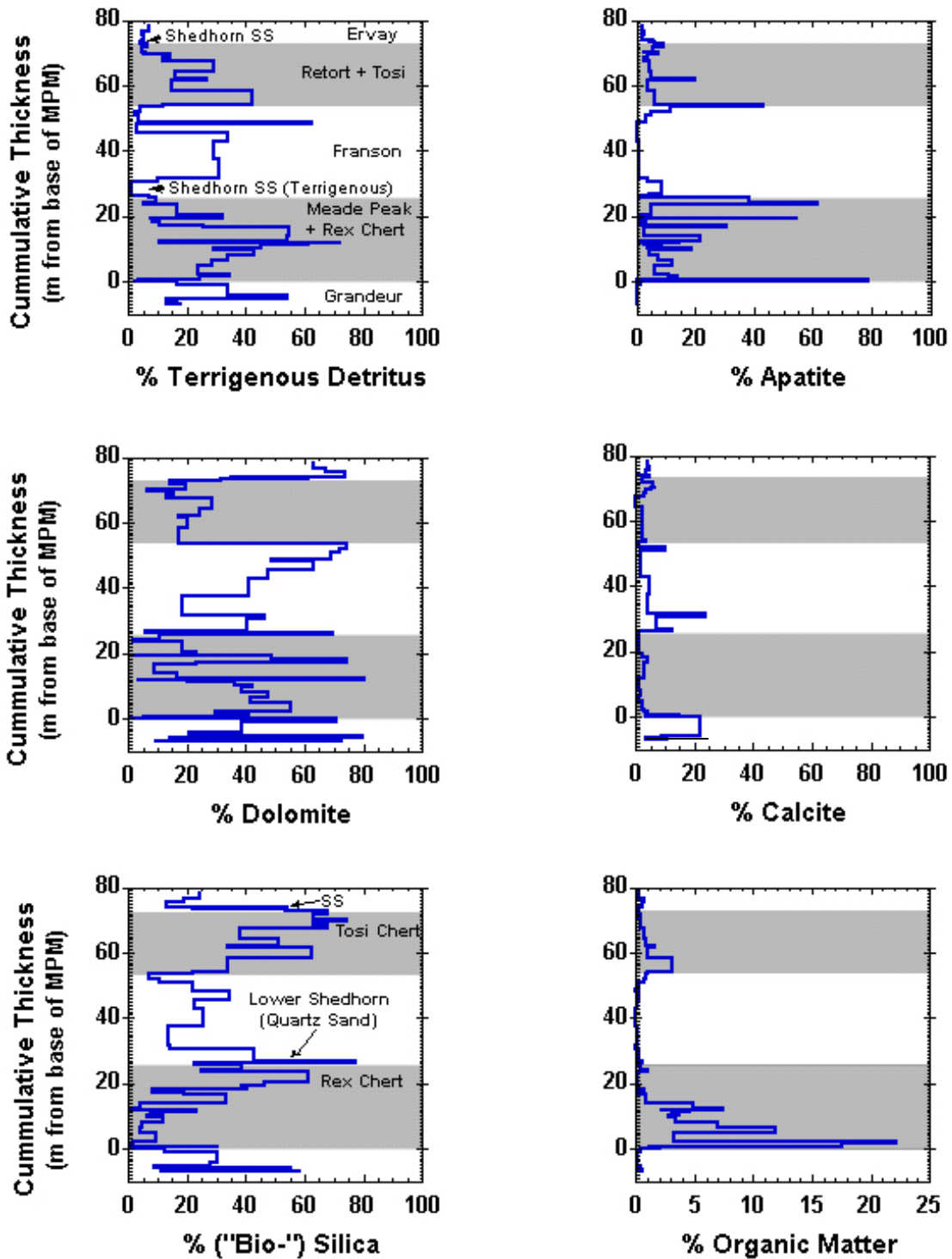


Figure 5. Variations in rock composition with stratigraphic position in the Lakeridge core. Component fractions determined from major-element oxide concentrations. Background shadings denote stratigraphic units. Missing core intervals (see fig. 3) split between overlying and underlying beds. Note difference in organic matter scale on x-axis; MPM is Meade Peak Member.

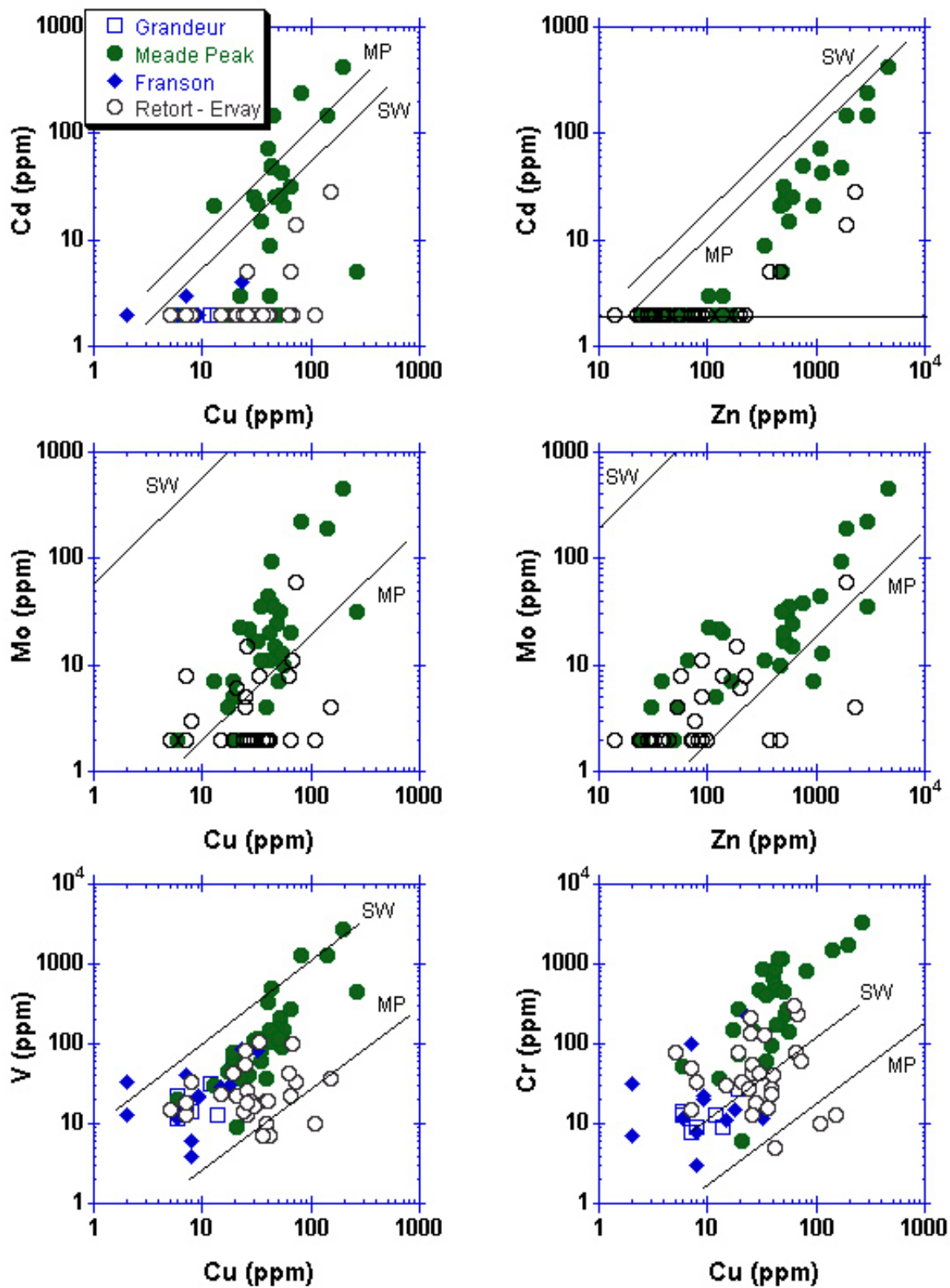


Figure 6. Scatter plots showing relationships between selected marine elements. Lines represent average ratios in modern deep seawater (SW) and modern marine plankton (MP).

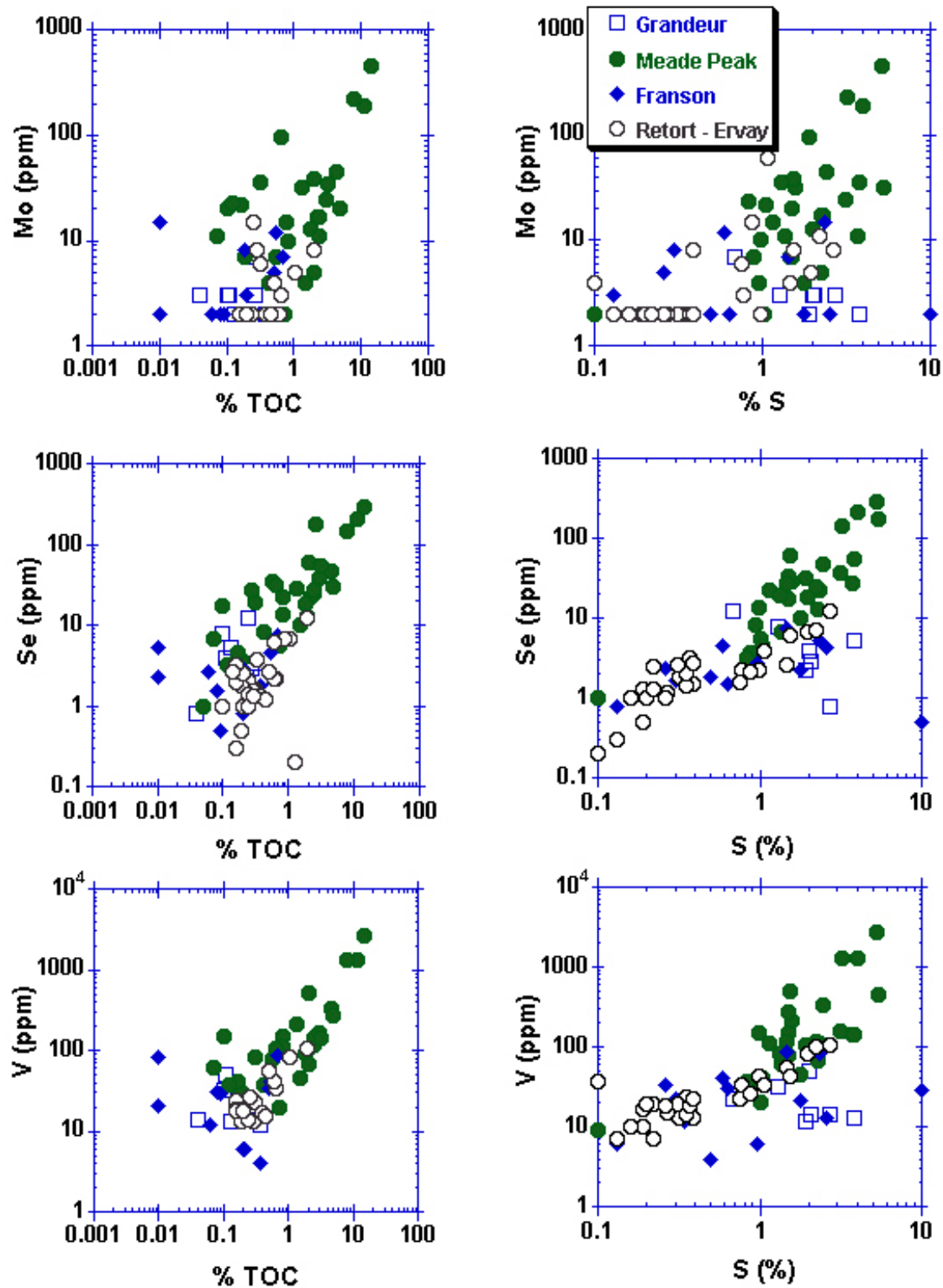


Figure 7. Scatter plots showing relationships between select marine elements and total organic carbon (TOC) and sulfur. Note sharp maxima lineation in points in element vs S plots.

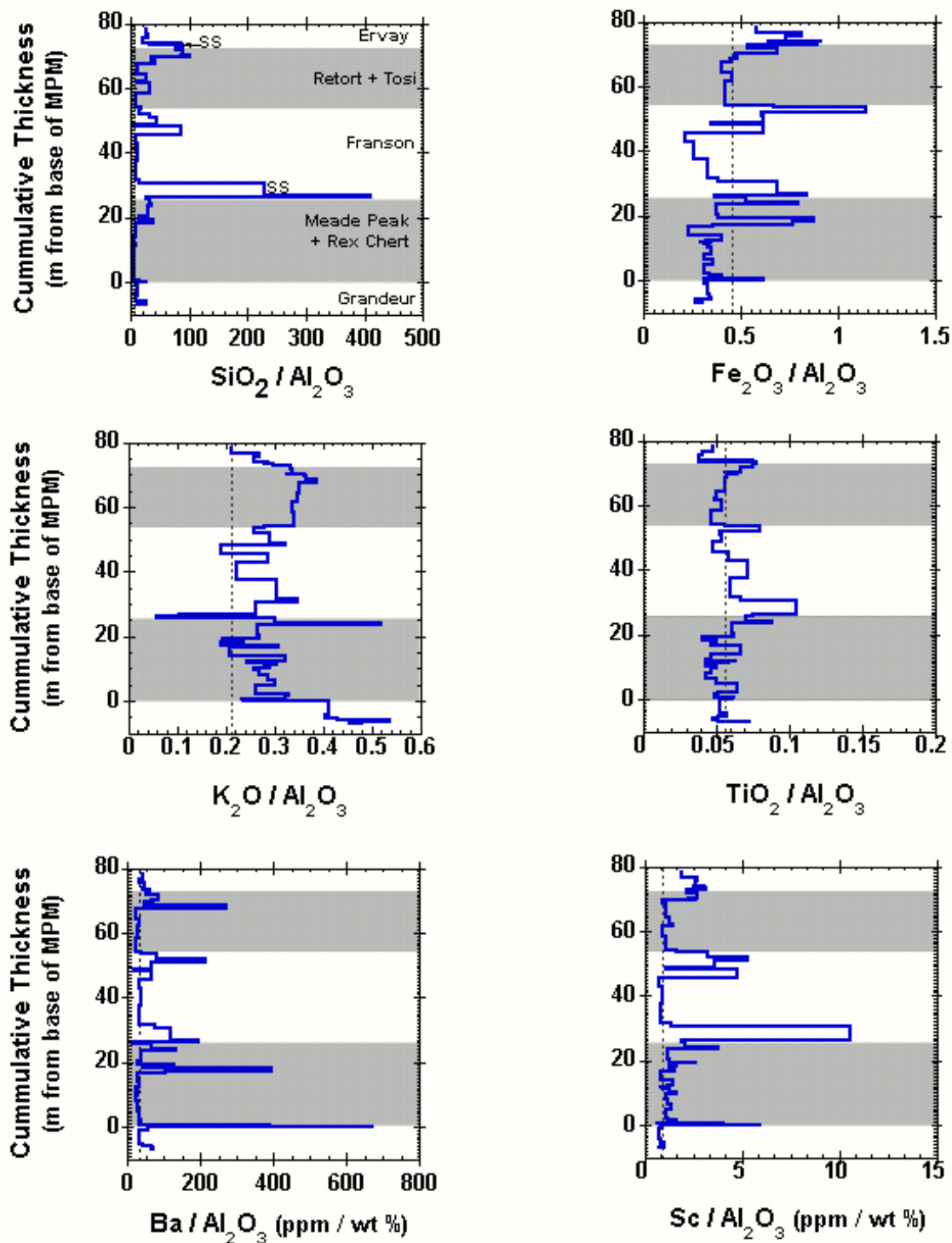


Figure 8. Variations in selected terrigenous element vs alumina ratios with stratigraphic position in the Lakeridge core. Dotted vertical lines denote major-element oxide ratios for world shale average (Turekian and Wedepohl, 1961; Wedepohl, 1969-1978). “SS” denotes Shedhorn Sandstone beds.

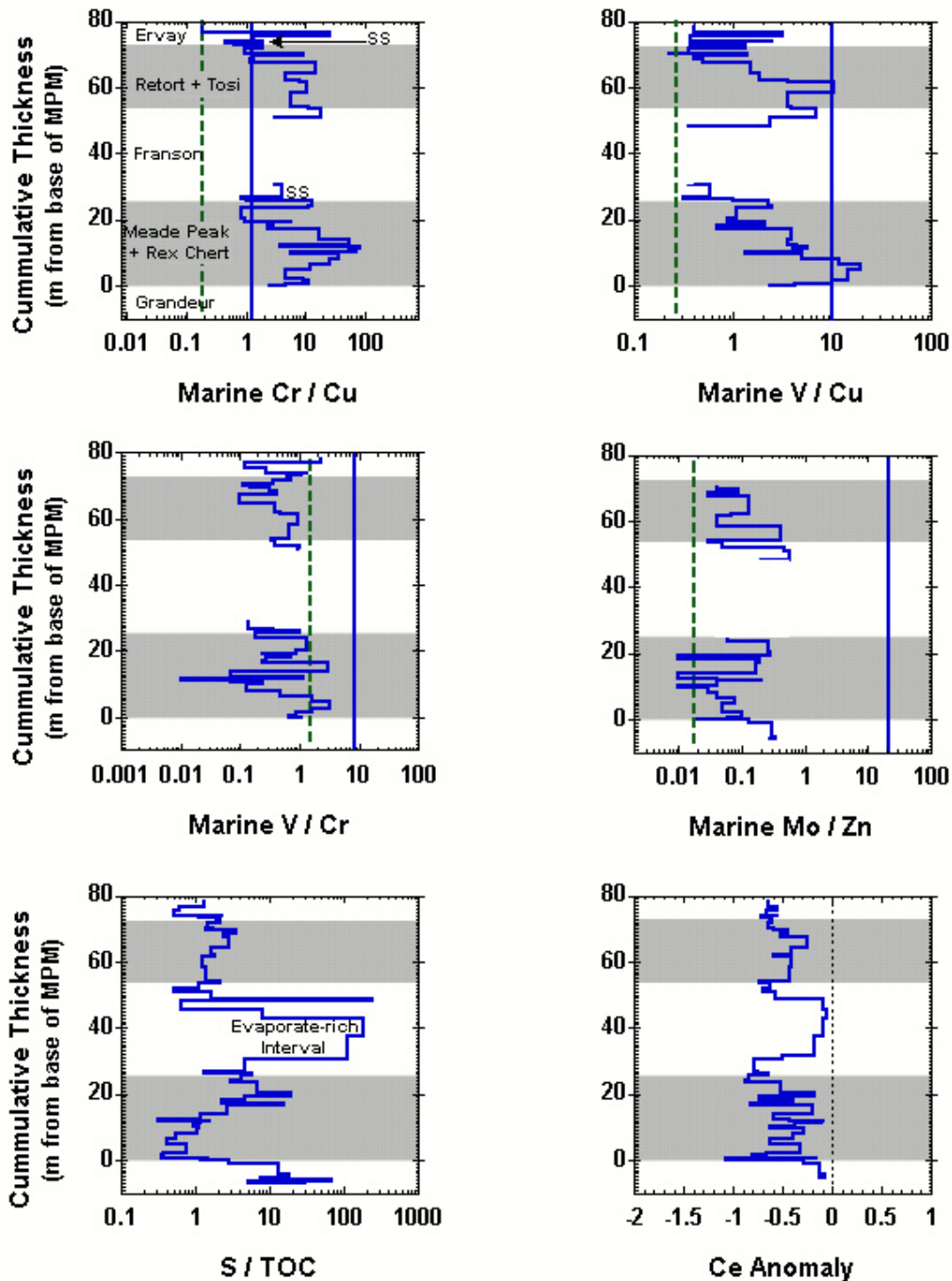


Figure 9. Variations in select marine element ratios and Ce anomalies with stratigraphic position in the Lakeridge core. Solid vertical lines denote seawater ratios; dashed vertical lines represent average marine plankton ratios (Martin and Knauer, 1973; Collier and Edmond, 1984; Collier, 1985; Brumsack, 1986); dotted vertical line represents WSA value for REEs (Piper, 1974). Blank areas (e.g., in Franson) represent intervals in which total concentration of one or both elements was below detection limits or marine fractions were insignificant. “SS” denotes Shedhorn Sandstone beds.

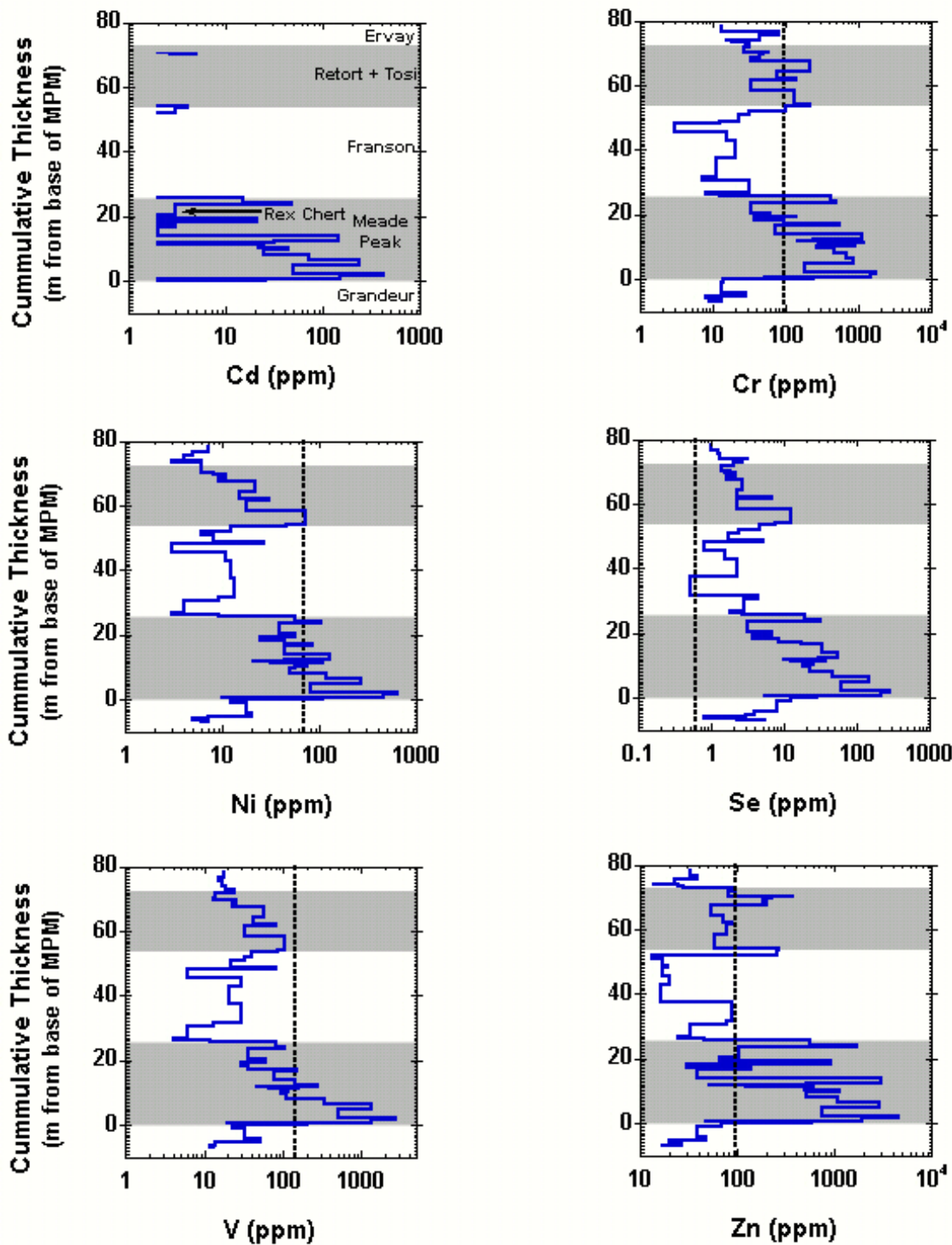


Figure 10. Variations in selected trace element concentrations with stratigraphic position in the Lakeridge core. Dotted vertical lines represent world shale average (Turekian and Wedepohl, 1961; Wedepohl, 1969-1978). Blank areas in Cd plot are intervals where Cd concentrations were below detection limits.